MK2 deficiency decreases mortality during the inflammatory phase after myocardial infarction in mice

Joëlle Trépanier[a,b], Sherin A. Nawaito[a,c,f], Pramod Sahadevan[a,b], Fatiha Sahmi[a], Natacha Duquette[a], Danielle Gélinas[a], Marc-Antoine Gillis[a], Yanfen Shi[a], Cynthia Torok[a], Marie-Élaine Clavet-Lanthier[a]. Matthias Gaestel[e], Martin G. Sirois, Jean-Claude Tardif[a,d], Bruce G. Allen[a,b,c,d]

From: Montreal Heart Institute, 5000 Belanger St., Montréal, Québec, Canada, H1T 1C8[a]. Departments of Biochemistry and Molecular Medicine[b], Pharmacology and Physiology[c], Medicine[d], Université de Montréal, Montréal, Québec, Canada, H3C 3J7. Institute of Cell Biochemistry, Hannover Medical School, Carl-Neuberg-Strasse 1, 30625 Hannover, Germany[e]. Department of Physiology, Faculty of Medicine, Suez Canal University, Ismailia, Egypt[f].

Running title: MK2-deficiency increases survival in mice post-MI

Address correspondence to:

Bruce G. Allen

Montreal Heart Institute, 5000 Belanger St., Montréal, Québec, Canada, H1T 1C8.

Telephone: (514) 376-3330 (3591).

FAX: (514) 376-1355.

E-mail: bruce.g.allen@umontreal.ca

Word Count: 13,684

Abstract

Background: Altering the onset, intensity, or duration of inflammation can impact the recovering heart's structure and function following myocardial infarction (MI). Substrates of MAP kinase-activated protein kinase 2 (MK2) include proteins that regulate the stability of AU-rich transcripts, including those of several pro-inflammatory cytokines. This study was to determine if MK2-deficiency impaired the inflammatory phase of post-MI wound repair.

Methods and Results: Myocardial infarctions were induced by permanent ligation of the left anterior descending coronary artery in 12-week-old male $MK2^{+/+}$ and $MK2^{-/-}$ littermate mice. Five days post-MI, survival was 100% in MI-$MK2^{-/-}$ (n = 20) and 79% in MI-$MK2^{+/+}$ mice (n = 29; Mandel-Cox test: $P < 0.05$). Area at risk and infarct size were similar. Echocardiographic imaging revealed that both systolic and diastolic LV diameters were greater in MI-$MK2^{+/+}$ than MI-$MK2^{-/-}$ mice. MK2-deficiency did not affect the increase in wall motion score index. Infiltration of neutrophils or monocytes did not differ significantly. Cytokine and chemokine transcripts were quantified in infarcted and non-infarcted LV tissue using qPCR arrays (QIAGEN). Three days post-MI, *Ifna2* was increased and *Il16* was decreased in infarcted tissue from $MK2^{-/-}$ hearts, compared with infarcted $MK2^{+/+}$ tissue, whereas in the non-infarcted $MK2^{-/-}$ myocardium *Il27* increased and *Tnfsf11*, *Ccl3*, and *Il1rn* were decreased. Five days post-MI, *Ctf16* and *Il10* increased in infarcted $MK2^{-/-}$ tissue whereas in the non-infarcted $MK2^{-/-}$ myocardium *Ccl9, Nodal, and Xcl2* increased and *Il15* decreased.

Conclusions: The findings of this study suggest MK2-deficiency is an advantage during the inflammatory phase of cardiac wound repair post-MI.

Keywords: MAPK-activated protein kinase-2, MK2, heart, myocardial infarction, cytokine, inflammation

Clinical Perspective

What is new?

-The effects of MAP kinase-activated protein kinase 2 (MK2) deficiency on survival, cardiac structure and function, and the inflammatory phase of wound healing following myocardial infarction were assessed using a constitutive, pan MK2-null mouse model.

-MK2-deficiency reduced mortality but did not alter area at risk or infarct size post-myocardial infarction. Inflammatory cell infiltration was also unaffected.

-MK2-deficiency altered the abundance of several cytokines (increased, decreased) in infarcted and non-infarcted myocardium post-MI.

What are the clinical implications?

-The initial phase of wound repair post-MI involves inflammation.

-The risk of damage to the myocardium and mortality may be reduced by inhibition of MK2 activity during the inflammatory phase of wound healing post-MI.

Introduction

Myocardial infarction (MI) results from the partial or total occlusion of a coronary artery, which leads to necrosis and irreversible damage to the heart [1-4]. Specifically, the lack of oxygen and nutrients causes a loss of cardiomyocytes (CM). As myocytes cannot replicate at the scale required to maintain muscle mass, they must be replaced by formation of a scar [1, 2]. Inflammation is the first phase of the post-MI healing process and is key to the subsequent healing phases, proliferation and maturation [3, 5], as it orchestrates immune cell recruitment and fibroblast activation to myofibroblasts as well as the clearance of extracellular matrix (ECM) and cell debris, all of which are crucial to the formation of new scar tissue [1, 3, 5-7]. Initially, necrosis results in the release of various signaling molecules such as TNF-α, IL-1 and other damage-associated molecular patterns (DAMPs), which trigger the activation of the immune system [6, 8, 9]. Neutrophils are the first immune cells attracted in the ischemic area [10]. They then actively participate in the recruitment of circulating monocytes and their activation to pro-inflammatory M1 macrophages [10]. M1 macrophages and neutrophils clear the cellular and ECM debris by both phagocytosis and secretion of various proteases [3, 4, 6]. They also secrete numerous cytokines including osteopontin (SPP1), granulocyte-macrophage colony-stimulating factor (CSF2), and adhesion molecules that participate in amplifying the recruitment of additional activated cells [3, 6, 11-17]. This cascade of signals promotes fibroblast migration into the infarct, where they activate to myofibroblasts and secrete ECM components [3, 4, 6]. Through this process of reparative fibrosis, a collagen scar is formed that both replaces the lost myocytes and permits the affected myocardium to withstand the pressure of the contracting heart without rupturing [3, 5, 10, 18].

Since inflammation initiates the post-MI healing process, alteration of the onset, intensity or duration of this response can have dramatic consequences on the heart's structure and function following MI. A robust inflammatory response can induce excessive secretion of cytokines and proteases [3], resulting in additional myocyte loss and degradation of the ECM [19-22], further weakening the ventricular wall, leading to thinning of the wall and dilatation [3, 19, 21-23]. In such

cases, ventricular rupture is more likely as the ventricular wall is no longer able to withstand the pressure developed during cardiac contractions [3, 19, 21-23]. Myocardial rupture could also occur if the inflammatory response is too weak to trigger reparative fibrosis [24, 25]. In this case, the migration of fibroblasts into the ischemic area and activation to myofibroblasts would be insufficient, leaving the wall in a weakened state and prone to rupture [24]. A prolonged inflammatory response can promote interstitial fibrosis formation, which would dramatically alter cardiac structure and function [3, 5, 11, 23], increasing LV wall stiffness and impairing myocyte synchronization [24, 26-28], leading to life-threatening conditions such as arrhythmias and heart failure [3, 26, 28, 29]. Various mechanisms exist to resolve the inflammatory response in a timely manner, such as a shift from recruitment of Ly-6C^{hi} monocytes to Ly-6C^{lo} monocytes and macrophage M2 polarization [30-32]. M2 macrophages secrete anti-inflammatory, pro-angiogenic and profibrotic factors such as IL-10 and TGF-β [5, 6, 31, 33]. However, if these resolving mechanisms are hindered, inflammation will be prolonged [27, 31] and excessive neutrophil and M1 macrophage activity will lead to a scar expansion [27, 31]. Thus, alterations in the coordinated events comprising the inflammatory phase of post-MI wound repair can have detrimental effects on the healing process that alter the structural integrity and functionality of the heart.

MAP kinase-activated protein kinase 2 (MK2) is a protein serine/threonine kinase that is activated by p38α and p38β MAPKs [34-37]. The three-tiered classical MAPK cascade amplifies the signal initiated by extracellular stimuli, such as tissue damage or an infection, leading to an appropriate cellular response [38-42]. These responses may include migration, proliferation, and differentiation, as well as regulation of the innate and adaptive immune system [38-40, 43]. Many roles have been attributed to MK2, including remodeling of the actin cytoskeleton, apoptosis, regulation of transcription factors, and genomic stability [36, 43-45]. MK2 is also a significant regulator of inflammation, as its inactivation is associated with decreased production of cytokines such as TNF-α, IL-1β, IL-6, IL-10, and INF-γ following a lipopolysaccharide (LPS) challenge in experimental models such as MK2-deficient mice, isolated splenocytes, and macrophages [40, 43, 46-48]. MK2

regulates the stability of numerous pro-inflammatory cytokine transcripts through phosphorylation of RNA-binding proteins such as tristetraprolin (TTP), AU-binding factor 1 (AUF1), and human antigen R (HuR) [43, 49]. Phosphorylation alters the affinity of these RNA binding proteins for the AU-rich elements in the 3'-UTRs of various mRNAs [43, 49]. Protein binding to the 3'-UTR is a determinant of stability and thus alters the half-life of the mRNA [43, 49]. In resting cells, TTP binding destabilizes target transcripts such as CSF2, IL-1, TNF-α, and IL-6, which continuously inhibits activation of the inflammatory response [36, 43, 48, 50]. MK2-mediated phosphorylation of TPP at Ser-82 and Ser-178 reduces its affinity for its target mRNAs and allows HuR to bind and stabilize these transcripts [43, 44, 48-51]. The resulting increase in transcript stability permits translation of various pro-inflammatory cytokines and ultimately triggers inflammation [43, 44, 48-51]. Thus, MK2 deficiency in mice alters the inflammatory response and reduces mortality post-LPS challenge [40, 43, 46-48, 52, 53]. *In vivo*, MK2-deficiency increases resistance to collagen-induced arthritis [54] and reduces atherosclerosis in hypercholesterolemic ($Ldlr^{-/-}$:$Mk2^{-/-}$) mice [55].

The acute, cardiomyocyte-specific activation of p38α in adult mice results in cardiomyocyte hypertrophy, interstitial fibrosis, contractile dysfunction, and mortality within one week [53]. Although such studies suggest p38 would be a suitable target for drug development, several p38α inhibitors have failed as treatments against inflammatory diseases due to their high toxicity and lack of long-term efficacy [43, 50, 56-58]. Furthermore, although targeted inactivation of p38α in platelets protected cardiac function after permanent ligation of the coronary artery [59], inactivation of p38α in cardiac fibroblasts led to 100% mortality in mice [26]. Thus, downstream targets of p38, such as MK2, may serve as more suitable targets for drug development that would circumvent the issues associated with direct inhibition of one or more p38 isoform [43, 56]. MK2-deficiency attenuates the hypertrophic effect and prevented the early mortality induced by cardiomyocyte-specific activation of p38 [53] whereas hypertrophy secondary to a chronic increase in afterload is delayed [60]. In addition, MK2-deficiency prevents or delays the development of a diabetic cardiomyopathy in a mouse model of type 2 diabetes [56, 61]. Since a proper inflammatory response

is key to effective wound repair post-MI and MK2 is an important modulator in inflammation, this study was undertaken to assess the consequences of MK2 deficiency on mortality during the inflammatory phase of reparative fibrosis post-MI in mice.

Material and Methods

Reagents for sodium dodecyl sulfate–polyacrylamide gel electrophoresis (SDS-PAGE), nitrocellulose membranes, and Bradford protein assay were from Bio-Rad Laboratories. Leupeptin and phenylmethylsulfonyl fluoride (PMSF) were from Roche Molecular Biochemicals. Rabbit polyclonal antibodies against p38α (# C-20) and MK2 (# 3042S) were from Santa Cruz Biotechnology and Cell Signaling Technology, respectively. Mouse monoclonal antibodies against GAPDH (glyceraldehyde 3-phosphate dehydrogenase) (# 4300) were from Ambion. Secondary antibodies conjugated with horseradish peroxidase were from Jackson ImmunoResearch Laboratories. Other reagents were either of analytic grade or the best grade available. The primers used for quantitative polymerase chain reaction (qPCR) reactions **(Table 1)** were produced by Invitrogen and their efficacy was previously demonstrated [62].

Mice. MK2-deficient mice ($MK2^{-/-}$) were generated by insertion of a neomycin resistance gene, which contains an in-frame translation stop codon, into the exon containing the catalytic subdomains V and VI of the protein [46]. The result is an inactive MK2 protein truncated at the active site. Twelve-week-old male $MK2^{+/+}$ and $MK2^{-/-}$ littermate mice were used for these experiments. $MK2^{-/-}$ mice do not display any adverse physiological or behavioral defects [36]. They are viable and fertile [36]. All experiments were approved by the local ethics committee and performed according to the guidelines of the Canadian Council on Animal Care. The mice were housed in a specific pathogen-free facility maintained at a constant room temperature and with a 12-hour light/dark cycle.

Myocardial infarction. Myocardial infarction (MI) was induced by permanent ligation of the left anterior descending coronary artery (LAD) as described previously [63]. Briefly, mice received an intraperitoneal injection of buprenorphine (0.1 mg/kg) before surgery and were then anesthetized with 2% isoflurane (in pure oxygen, 1 L/min). For post-operative analgesia, buprenorphine was administered 6 to 8 h after the procedure and again the next morning.

Myocardial infarction was achieved by permanent ligation of the left anterior descending coronary artery with a 10-0 nylon surgical suture (Ethicon). The ligature was placed 1 mm below the left atria. Mice in the sham groups went through the same procedure but did not have a ligature on their artery. The surgeon was blinded to the genotype of the animals. Surviving mice were euthanized 3- or 5-days post-surgery. Cardiac structure and function were evaluated by transthoracic echocardiographic imaging on the day before the surgery or on the morning of the procedure and again prior to sacrifice.

Determine the area at risk and infarct size. To determine the possible effects of MK2-deficiency on the area at risk (AAR) and infarct size, separate groups of wild-type and MK2-deficient mice underwent LAD ligation and were perfused with 2% Evans blue dye 30 min after ligation. Hearts were then removed, washed in 0.9% saline, and trimmed of atria and adipose tissues. Hearts were then wrapped in plastic wrap, placed in a -80 °C freezer for 5 min, cut into 4-5 transversal sections of 2 mm thickness, photographed, incubated for 20 min in 1% 2,3,5-triphenyl tetrazolium chloride (TTC) in PBS at 37 °C, fixed using 10% formalin in PBS, and photographed again to reveal the infarct area within the AAR. The AAR was the area not stained with Evans blue and was expressed as a percentage of the total left ventricular (LV) area. The infarct area (IA) was the area not stained in red by TTC and was expressed as a percentage of the AAR.

Diagnosis of heart rupture. All non-surviving mice underwent a necropsy to identify the cause of their death. Death due to heart rupture was diagnosed as the presence of coagulated blood around the heart and in the chest cavity.

Transthoracic echocardiography and calculations. Echocardiographic imaging was performed on mice anesthetized with 2% isoflurane (in pure oxygen, 1 mL/min) within 24 h of surgery and immediately before sacrifice. Images were acquired using a Vivid 7 Dimension system (GE Healthcare, Horten, Norway) and a i13L probe (10-14 MHz) by a technician who was

blinded as to the genotype of the mice. The measurements obtained are the average of three consecutive cardiac cycles. Echocardiographic imaging of LV structure and function were as described previously [63, 64]. Two-dimension echocardiography was used to visualize the MI. Left ventricular anterior wall thickness at end cardiac diastole ($LVAW_d$) and LV posterior wall thickness at end cardiac diastole ($LVPW_d$) as well as the LV dimension at end cardiac diastole (LVD_d) and at end cardiac systole (LVD_s) were measured using a parasternal short-axis view at the level of the papillary muscles by using M-mode echocardiography. Left atrium dimension at end cardiac systole (LAD_s) and diastole (LAD_d) were also measured using the same mode. These parameters were then used to calculate the LV mass (LV_{mass}) using this equation: $1.055 \cdot ((LVD_d + LVAW_d + LVPW_d)^3 - (LVD_d)^3)$. The parameters were also used to calculate the fractional shortening (FS) by using the following equation: $(LVD_d - LVD_s) / LVD_d \cdot 100\%$ [65]. The formula available in the Vivid 7 operating system was used to calculate the LV ejection fraction (EF). LV regional contractility was assessed by using tissue Doppler imaging (TDI) to determine basal lateral wall systolic contractile velocity (S_L) and basal septum systolic contractile velocity (S_S). Pulsed wave Doppler was used in apical four-chamber view to obtain various LV diastolic parameters such as the trans mitral flow (TMF), the early filling deceleration time (EDT), the early filling deceleration rate (EDR), the mitral valve closure to opening time (MV_{CO}), the trans-mitral early (E) and late atrial (A) filling velocities. Pulsed-wave Doppler was used to obtain the LV ejection time (LVET) by measuring the time starting from the beginning to the end of the LV outflow. These measurements were used to calculate the global myocardial performance index (global MPI) by using the following formula: $(MV_{CO} - LVET) / LVET \cdot 100\%$. The systolic flow of pulmonary venous flow (PVF) (S) and the diastolic flow of PVF (D) were both also obtained using the pulsed wave Doppler. The mitral annulus was viewed by TDI to measure velocities during early filling on the septal segment (septal E_m) and lateral segment (lateral E_m) as well as the atrial filling for the septal (septal A_m) and the lateral (lateral A_m) segments. These parameters were used to calculate values for lateral and septal E/E_m. The images taken by pulsed-wave Doppler in apical five-chamber view were used to determine the isovolumetric relaxation time (IVRT). As

MK2-deficient mice are bradycardic, the heart rate-corrected IVRT was calculated as follows: corrected IVRT (IVRTc) = IVRT / $RR^{1/2}$. The RR interval was acquired using simultaneously recorded ECG. The septal and lateral MPI were calculated using the following equation (b − a) / a · 100%. The value identified as "a" is the interval of time from the start to the end of the S_L or S_S for lateral and septal MPIs, respectively. Similarly, "b" corresponds to the interval of time from the end of A_m to the beginning of E_m measured at the lateral and septal annular segments for lateral and septal MPIs, respectively. LV wall motion was scored using a scale numbered from 1 to 5 : 1 = normal, 2 = hypokinesis, 3 = akinesis, 4 = dyskinesis and 5 = aneurysmal. The wall motion score index (WMSI) was calculated by using the following equation: sum of all scores / number of segments viewed. Right ventricular (RV) diameter at end diastole (RVD_d), RV anterior wall thickness at end diastole ($RVAW_d$) and tricuspid annulus plane systolic excursion (TAPSE) were measured using M-mode echocardiography. Pulsed wave Doppler was used to obtain the acceleration time (AT) and RV ejection time (RVET) of the pulmonary artery flow. The same method was used to evaluate trans-tricuspid flow early filling velocity (E_t), late (atrial) filling velocity (A_t), early filling deceleration rate (E_tD rate), early filling deceleration time (E_tDT), and tricuspid valve closure to opening time (TV_{CO}). Tissue Doppler imaging of the tricuspid annulus was used to measure the right ventricular lateral wall peak systolic velocity (S_R), lateral tricuspid annulus peak velocity during early filling (E_m), and lateral tricuspid annulus peak velocity during late (atrial) filling (A_m). The RV MPI was calculated in the same manner as that of the LV.

Histological analysis. Mice were anesthetized with 2% isoflurane (in pure oxygen, 1 L/min), hearts removed, and perfused with a saline solution (0.9% sodium chloride and heparin 2 USP units/mL) to clear the blood in the arteries, followed by a second perfusion with 10% formalin. A transversal cut was then made between the ligature and the apex of the heart, and the two halves were then placed in a cassette and immersed in 10% formalin solution. Staining and collagen quantification were performed in the histology facility in the laboratory of Dr. Martin G. Sirois at the Montreal Heart Institute by a histology technician blinded to the genotype of the sample.

Following a 24 h fixation step in 10% formalin, hearts were dehydrated by immersion in solutions of increasing alcohol concentrations (70%, 95%, 100%), followed by xylene, embedded in paraffin, cut in 6 μm transversal sections, and mounted on charged slides. Sections from all mice in the study underwent histochemical and immunohistochemical assessment. In preparation for immunohistochemistry, tissue sections were treated with citrate buffer (pH 6.0) for antigen retrieval and 3% hydrogen peroxide solution to block endogenous peroxidase activities prior to blocking for 20 min in phosphate buffered saline (PBS) containing 10% serum (same species as secondary antibody). Sections were then incubated with primary antibody diluted in PBS containing 1% normal serum overnight in a humidified chamber at 4 °C. The primary antibodies used were a mouse monoclonal antibody against smooth muscle α-actin (α-SMA, a myofibroblast marker; A-2547, Sigma-Aldrich) and rabbit polyclonal antibodies against myeloperoxidase (MPO, a neutrophil and monocyte marker; ab65871, Abcam), CD206/mannose receptor (a macrophage marker; ab64693, Abcam), and CD31/PECAM-1 (an endothelial cell marker; sc-1506, Santa Cruz Biotechnology). The negative control groups were incubated in the absence of primary antibody. After washing, tissue sections were incubated with a biotin-conjugated secondary antibody for 30 min, washed again, and incubated with horseradish peroxidase-conjugated streptavidin (Vector Labs) for 30 min. Immunoreactivity was visualized using the chromogenic peroxidase substrate 3,3'-diaminobenzidine (Vector Labs). Finally, sections were counter-stained using hematoxylin and mounted using Permount. Images of the heart sections were taken at 4X and 20X using an Olympus BX46 microscope. Analysis of the infarct area as well as collagen quantification in the infarct area were performed using Image Pro Plus software version 7.0 (Media Cybernetics, Silver Spring, MD) and expressed as a percentage of the total tissue area of each section. Images of MPO-immunoreactivity were acquired at 20X magnification whereas those of CD206, CD31, or α-SMA immunoreactivity were acquired at 40X using an Olympus BX46 microscope.

Isolation and culture of cardiac ventricular fibroblasts. Fibroblasts were isolated from male $MK2^{+/+}$ and $MK2^{-/-}$ mice aged between 11 to 13 weeks as described previously [63, 64, 66]. Mice were

sacrificed by exsanguination following a pentobarbital injection. Hearts were removed and immediately immersed in sterile PBS (137 mM NaCl, 2.7 mM KCl, 4.2 mM $Na_2HPO_4 \cdot H_2O$, pH 7.4) at 37 °C. After removing the atria and adipose tissue, the ventricles were cut into pieces of approximately 1 mm^2, which were then subjected to a series of digestions in a dissociation medium (116.4 mM NaCl, 23.4 mM HEPES, 0.94 mM $NaH_2PO_4 \cdot H_2O$, 5.4 mM KCl, 5.5 mM dextrose, 0.4 mM $MgSO_4$, 1 mM $CaCl_2$, 1 mg/mL BSA, 0.5 mg/mL collagenase type IA, 1 mg/mL trypsin, 0.020 mg/mL pancreatin, pH 7.4). with gentle shaking on an orbital mixer placed in a humidified incubator at 37 °C under a 5% CO_2 atmosphere. After 10 minutes, the supernatant, containing the cells released from the tissue, were collected, and centrifuged at 1500 rpm for 5 min. After 10 cycles of digestion and centrifugation, the cell pellets were resuspended in 4 mL of Medium 199 (M199, Sigma-Aldrich) supplemented with 10% FBS, 2% antibiotics (streptomycin and penicillin, Hyclone) and 2% amphotericin B (Gibco), plated onto two 35 mm petri dishes, and incubated in a humidified incubator at 37 °C in a 5% CO_2 atmosphere. The media was changed after 150 minutes, to remove cell debris, and again the following morning. These cells were referred to as passage 0.

Scratch-wound assays. Fibroblast motility was assessed by scratch-wound assay in passage 0 fibroblasts cultures. Fibroblasts were seeded directly in 12 well plates and the media was changed every 24 h until cultures reached 80% confluence. Cells were then washed with PBS and maintained in serum-free M199 for 18 h. A scratch was created across the center of each well with a P1000 pipette tip and the plates were washed with PBS to remove the debris. Different treatments were used: serum-free media, media containing serum, and media containing serum and angiotensin II. Images were acquired immediately after creating the scratch (time zero) and again 24 h later using a Nikon ELWD 0.3/OC 75 camera (magnification of 4X). ImageJ version 1.48 was used to assess the percentage of the open wound remaining after 24 h.

RNA extraction and RT^2 Profiler PCR Arrays. The LV tissue from infarcted hearts was separated into healthy and infarcted tissue. The LV from sham mice was left intact. Tissue

samples were then submerged in 2-methylbutane, snap frozen with liquid nitrogen, and stored frozen at -80 °C until further analysis. In preparation for RNA extraction, frozen tissue was pulverized to a fine powder under liquid nitrogen using a mortar and pestle. Powdered tissue was combined with 500 µL of TRIzol reagent and homogenized with a single 10 s burst using a Polytron PT 2100 homogenizer. Total RNA was then purified using RNeasy Mini Kits (QIAGEN Inc.) according to the manufacturer's instructions. The concentration and purity of each RNA sample were evaluated using a NanoDrop ND-1000 spectrophotometer and only the samples with a 260/280 absorbance ratio above 1.8 were used. First strand cDNA was synthesized from 0.5 mg of total RNA using QIAGEN RT^2 First Strand Kits and transcripts for mouse cytokines and chemokines were quantified using qPCR microarrays comprising 96-well plates precoated with primers (QIAGEN PAMM-150Z). Each 96-well plate also contained primers for 5 housekeeping genes as well as positive and negative controls. qPCR was performed using an ABI StepOnePlus instrument according to the instructions provided by the manufacturer. Data was analyzed according to the instructions provided in the RT^2 Profiler PCR Array Data Analysis v3.5 Handbook using the software on the QIAGEN website (https://dataanalysis.sabiosciences.com/pcr/arrayanalysis.php) and normalized to internal controls. Changes were considered significant when $P < 0.05$.

Statistical analysis. Normality tests (Shapiro-Wilk) were performed on all data. The Mandel-Cox test was used to analyze survival curves. Data are presented as mean ± SEM or median (1st quartile, 3rd quartile). For multiple comparisons of means involving a combination of 2 independent factors such as surgery (LAD ligation, sham) or genotype (MK2$^{+/+}$, MK2$^{-/-}$), 2-way ANOVA followed by Tukey's post hoc tests were performed. When a lognormal distribution was indicated, data was log-transformed before conducting the ANOVA. All tests were two-sided. A P value < 0.05 was considered significant. Statistical analyses were performed using Prism version 9.4.1 for Mac OS X (GraphPad Software, La Jolla, CA).

Results

MK2-deficiency decreased mortality after LAD ligation. Through phosphorylation of RNA-binding proteins, MK2 regulates the stability of several cytokine transcripts [43, 46]. As the first phase of wound-healing post-MI involves an inflammatory response, we assessed the effects of an MK2-deficiency on the inflammatory phase of post-MI wound healing. Myocardial infarctions were induced by permanent ligation of the left anterior descending coronary artery and mice were sacrificed on the third or fifth day following the surgery, which roughly corresponds to the middle and the end of the inflammatory response. All sham-operated ($MK2^{+/+}$: 39/39; $MK2^{-/-}$: 38/38) and ligated mice ($MK2^{+/+}$: n = 45/45; $MK2^{-/-}$: n = 41/41) survived to day 3 post-MI **(Figure 1A)**. However, 5 days post-MI, survival of $MK2^{-/-}$ mice was significantly greater (100%, n = 21/21) than $MK2^{+/+}$ mice (79%, n = 23/29, Mandel-Cox test: $P = 0.0285$) **(Figure 1B)**. Post-mortem examinations revealed that all deaths in MI-$MK2^{+/+}$ mice occurring on days 3 - 5 were due to heart rupture, as determined by both the accumulation of blood in the chest cavity and the presence of a clot on the heart [67]. In addition, one MI-$MK2^{+/+}$ mouse had to be sacrificed on day 4 as it was in distress. A similar number of $MK2^{+/+}$ and $MK2^{-/-}$ mice did not survive the first hour after the surgery ($MK2^{+/+}$: n = 3; $MK2^{-/-}$: n = 2). These 6 mice were excluded from the study. Hence, mortality was reduced in MK2-deficient mice during the inflammatory phase of post-MI wound healing.

MK2-deficiency did not alter the area at risk or infarct size. We examined the possible effect of an MK2-deficiency on the size of the area at risk (AAR) following LAD ligation by infusing a group of $MK2^{+/+}$ and $MK2^{-/-}$ mice with Evans blue dye, which is excluded from the AAR, 30 min after ligation. MK2-deficiency had no effect on the size of the AAR [expressed as a percentage of left ventricular (LV) area ($MK2^{+/+}$: 22.8 ± 2.5%, n = 6; $MK2^{-/-}$: 19.2 ± 5.1%, n = 9; $P > 0.05$: **Figure 1C**)]. Similarly, 2,3,5-triphenyl tetrazolium chloride (TTC), which stains viable myocardium, revealed that, after 30 min of ligation, infarcts were of similar size in $MK2^{+/+}$ and

MK2$^{-/-}$ mice [expressed as a percentage of AAR (MK2$^{+/+}$: 57.5 ± 10.7%, n = 6; MK2$^{-/-}$: 39.5 ± 5.3%, n = 9; $P > 0.05$: **Figure 1D**)].

MK2-deficiency attenuated LV dilation post-MI. The effects of MK2-deficiency on LV and RV structural and functional remodeling post-MI were assessed by echocardiographic imaging **(Tables 1 and 2)**. Generally speaking, three- and five-days post-MI, certain genotype-specific differences were detected in the structural or functional alterations resulting from MI. Both MK2$^{+/+}$ and MK2$^{-/-}$ mice displayed reduced LV (ejection fraction) and RV (tricuspid annular plane systolic excursion) systolic function, left atrial (LA) dilation, increased wall motion score index (WMSI), and increased (indicating poorer performance) in LV and RV myocardial performance indices. Tissue Doppler imaging revealed little genotype-dependent effect on the MI-mediated changes in mitral annulus velocity: the exception being the peak systolic velocity of the septal segment (S_S), which was reduced in MI-MK2$^{-/-}$ mice, relative to MI-MK2$^{+/+}$ mice, whereas the lateral segment velocity (S_L) was not significantly affected by the absence of MK2 **(Figure 2A and 2B)**. Note that in comparing structure, 12-week-old MK2-deficient mice were smaller than age-matched littermates **(Table 1)** [60]. However, 2-way ANOVA also revealed significant genotype x surgery interactions post-MI. The thickness of the LV posterior wall (LVPWd) was significantly increased in MI-MK2$^{-/-}$ but not MI-MK2$^{+/+}$ mice 5-d post-MI. Left ventricular internal diameter at end-diastole (LVD_d) and end-systole (LVD_s) were significantly smaller in MI-MK2$^{-/-}$ than MI-MK2$^{+/+}$ mice 5-d post-MI **(Table 1, Figure 2C and 2D)** as was LV volume at end-diastole (LVV_d) (**Figure 2E)**. Although the LV volume at end-systole (LVV_s) was also significantly smaller in MI-MK2$^{-/-}$ than MI-MK2$^{+/+}$ mice 5-d post-MI **(Table 1, Figure 2F)**, no interaction effect was detected ($P > 0.05$). Examining transmitral flow velocities during diastole showed early diastolic filling velocity (E) and the ratio of early to late diastolic filling velocities (E/A) were greater in MI-MK2$^{-/-}$ mice than MI-MK2$^{+/+}$ mice 3-d post-MI as was the peak upper pulmonary venous flow during diastole (upper D) (surgery x genotype interaction: $P < 0.05$). The deceleration time and deceleration rate of the early wave of diastolic filling (EDT, ED rate) as well

as heart rate-corrected isovolumetric relaxation time ($IVRT_c$) in MI-$MK2^{-/-}$ and MI-$MK2^{+/+}$ mice did not differ significantly. Similarly, the ratio of peak E wave velocity to mitral annulus peak velocity during early diastolic filling (E/E_m), an indicator of LV filling pressure, in MI-$MK2^{-/-}$ and MI-$MK2^{+/+}$ mice, did not differ significantly. These data suggest that the deficiency of MK2 attenuated LV dilation post-MI but was neither beneficial nor detrimental to cardiac systolic or diastolic function.

The absence of MK2 also altered remodeling of the RV post-MI. Although the group means for right ventricular internal diameter at end-diastole (RVD_d) did not differ significantly, there was a significant interaction effect 3-d post MI ($P < 0.05$): RVD_d increased in MI-$MK2^{+/+}$ mice, relative to sham-$MK2^{+/+}$ mice, whereas it decreased in MI-$MK2^{-/-}$ mice **(Table 2)**. The absence of MK2 also altered the effect of MI on transtricuspid flow early filling velocity (E_t) 3-d post-MI. In MI-$MK2^{+/+}$ hearts, E_t was increased, relative to sham mice, whereas it was decreased in MI-$MK2^{-/-}$ hearts. A similar effect was observed on the ratio of E_t to tricuspid annulus peak velocity during early diastolic filling (E_t/E_m). An interaction effect ($P < 0.05$) was observed for tricuspid E_m 5-d post-MI, which was actually a result of E_m in MI-$MK2^{+/+}$ hearts decreasing, relative to sham-$MK2^{+/+}$, to peak velocities observed in sham-$MK2^{-/-}$ and MI-$MK2^{-/-}$ mice. Tricuspid E_m was slower in sham-$MK2^{-/-}$ hearts and did not undergo further reduction as a result of MI.

MK2-deficiency did not alter infarct area size or collagen content 3- and 5-days post-MI. Reparative fibrosis post-MI involves the deposition of collagen to provide structural support to the LV wall [3]. Impaired collagen deposition can lead to thinning of the LV wall whereas excessive deposition can cause LV stiffness: both events can negatively affect heart function [3, 5]. The larger a scar area becomes, the more severely function is impaired [3, 5]. As a result, infarct size and collagen content are crucial determinants of the long-term outcomes post-MI. For histological analysis, hearts were first cut along the short axis, as shown in Figure 3A, resulting in upper (A) and lower regions (B) of the infarct **(Figure 3A)**. The upper sections allowed a better assessment of the scar border, whereas the lower sections permitted a better assessment of scar morphology.

Sections from both 'A' and 'B' were stained using Masson's trichrome, which colors healthy tissue red and collagen blue. MK2-deficiency did not alter the infarct area **(Figure 3B and 3C)** 3- or 5-days post-MI in either the upper (section A) or lower (section B) regions of the LV. As one would expect this early in the wound-repair process, the collagen content in the infarct area **(Figure 4)** was low 3 days post-MI and had increased slightly 5 days post-MI. In addition, 5 days post-MI, the collagen content in the infarct region of the 'A' sections was less in MI-MK2$^{-/-}$ than MI-MK2$^{+/+}$ mice **(Figure 4B)**.

MK2-deficiency did not affect neutrophil or macrophage recruitment to the infarct or peri-infarct regions. As the inflammatory phase of wound repair is essential for appropriate healing and the absence of MK2 did not result in increased mortality within the first 5-days post-MI, we next sought to characterize the effects of MK2-deficiency on the inflammatory response in infarcted hearts. Neutrophils and monocytes/M1 macrophages, the first responders to the inflammatory factors released by necrotic myocytes [20], begin to clear the debris caused by the ischemia and participate in the inflammatory response by secreting numerous cytokines [27, 64, 68]. To determine if the absence of MK2 affected the recruitment of neutrophils or monocytes to the infarct or peri-infarct regions, tissue sections were decorated with antibodies against myeloperoxidase (MPO). MPO immunoreactivity was sparse in the myocardium of sham hearts and the non-infarcted myocardium hearts from both MI-MK2$^{+/+}$ and MI-MK2$^{-/-}$ mice. The abundance of MPO immunoreactivity was greater in the peri-infarct and infarct regions, relative to both sham hearts and the non-infarcted myocardium of infarcted hearts; however, MPO immunoreactivity did not differ significantly between MK2$^{+/+}$ and MK2$^{-/-}$ mice 3- or 5-days post-MI **(Figure 5)**.

As the inflammatory response evolves, M1 macrophages shift to their M2 phenotype, which are then involved in resolving the inflammation and initiating tissue repair. The abundance of M2 macrophages, assessed by decorating tissue sections with anti-CD206 antibodies, was low in the myocardium of sham hearts and the non-infarcted myocardium of hearts from both MI-MK2$^{+/+}$

and MI-MK2$^{-/-}$ mice and greatest in the peri-infarct zone at both 3- and 5-days post-MI **(Figure 6)**. Interestingly, 5-days post-MI, in the 'A' sections, the abundance of CD206 immunoreactivity in the peri-infarct region of MI-MK2$^{+/+}$ hearts showed a trend towards being greater than in MI-MK2$^{-/-}$ hearts, but the difference did not reach significance. No genotype-dependent differences were observed in the 'B' sections.

MK2-deficiency did not alter the accumulation or distribution of myofibroblasts. The healing process following an MI involves formation of a collagen scar produced by fibroblasts that migrate into the affected area and become activated to myofibroblasts [5, 11]. A hallmark of myofibroblasts is the expression of α-SMA [26, 69]. Thus, α-SMA-specific antibodies were used to assess the abundance of myofibroblasts in transverse sections of infarcted and sham hearts **(Figure 7)**. α-SMA immunoreactivity was more abundant in the peri-infarct zone than in the non-infarcted and infarcted myocardium of MI hearts and the myocardium of sham hearts. However, MK2 -deficiency did not affect the distribution or intensity of α-SMA immunoreactivity. These results reveal a similar recruitment and activation of fibroblasts post-MI in hearts from wild type and MK2-deficient mice, suggesting the initiation of fibrosis was not affected by the absence of MK2.

Vascularization. Angiogenesis is an important component of wound repair in that it reduces myocyte mortality and maintains cardiac function by rebuilding the vasculature required to provide oxygen and nutrients to cardiac tissue [70-72]. As deletion of MK2 impedes angiogenesis in cutaneous wound repair [73] and colorectal cancer [74, 75], we next sought to assess the effect of MK2-deficiency on angiogenesis post-MI. First, immunohistochemical staining for CD31, an endothelial cell marker [76], was undertaken. In general, CD31 immunoreactivity was most abundant in the peri-infarct zone in 'A' and 'B' sections for both genotypes (**Figure 8A and 8B**). On days 3 and 5 post-MI, CD31 staining was greater in the peri-infarct zone of MI-MK2$^{-/-}$ hearts compared to that of MI-MK2$^{+/+}$ hearts in both 'A' and 'B' sections (**Figure 8A and 8B**). In addition, 5 days post-MI, CD31 staining was greater in the infarct zone of MI-MK2$^{-/-}$ hearts compared to that of MI-MK2$^{+/+}$ hearts in the 'B' sections (**Figure 8B)** and was associated with a significant surgery x

445 genotype interaction effect ($P < 0.05$). Thus, the absence of MK2 activity appeared to promote
446 the recruitment of CD31-positive endothelial cells to the infarct and peri-infarct zones.

447 We next examined if the absence of MK2 altered the density of vessels with a diameter of
448 20 μm or less in the infarct border region five-days post-MI using an immunohistological approach
449 with antibodies directed against CD31 and α-SMA. No α-SMA-positive vessels of this diameter
450 were detected **(Data not shown)**. However, the density of CD31-positive vessels with a diameter
451 of 20 μm or less was significantly reduced in the infarct border region of MI-MK2$^{-/-}$ hearts, relative
452 to MI-MK2$^{+/+}$ hearts, in the 'A' sections **(Figure 8C)**.

453 *The effects of an MK2-deficiency on cytokine production following an MI.* Known substrates
454 for MK2 include the RNA-binding proteins tristetraprolin (TTP), HuR, and ARE/poly(U)-
455 binding/degradation factor 1 (AUF1) [43, 49]. These proteins bind to AU-rich elements (ARE) present
456 in the 3'-untranslated region (UTR) of numerous mRNAs, including those of several pro-
457 inflammatory cytokines [43, 49], and either stabilize (HuR) or destabilize (TTP, AUF1) mRNA,
458 implicating MK2 in the post-transcriptional regulation of gene expression [43, 49]. MK2-mediated
459 phosphorylation of TTP and HuR has opposing effects on their binding to mRNA: TTP dissociates
460 from and promotes the stability of AU-rich mRNA whereas HuR binds to and stabilizes its target
461 mRNAs [43, 49]. Hence, we next examined the effect of MK2-deficiency on the abundance of
462 inflammatory cytokine mRNAs in healthy and infarcted cardiac tissue 3- and 5-days post-MI using
463 RT^2 Profiler PCR Arrays (QIAGEN PAMM-150Z; **Supplementary Tables 1 - 16**). These data,
464 normalized to the abundance of each transcript in the ventricular myocardium of wild type sham
465 mice, are summarized in the form of volcano plots in **Figure 9**. Due to space limitations, some,
466 but not all, mRNAs that underwent a 2-fold change in abundance with $P < 0.05$ are identified in
467 the figure. The inflammatory phase of repair starts within 12 hours of MI and can last up to 6 days
468 [3, 4, 6]. In mice, day 3 post-surgery corresponds roughly to the midpoint of the inflammatory phase
469 and the start of granulation tissue formation whereas day 5 corresponds to the resolution of the
470 inflammatory phase. Both the absence of MK2 and time after MI affected the abundance of

numerous transcripts in the sham, infarcted, and non-infarcted myocardium. It is also worth noting that the abundance of *Il15* mRNA was reduced in MK2-deficient sham hearts **(Figure 9)**.

The absence of MK2 impairs the induction of several cytokines in cells and mice in response to lipopolysaccharide (LPS) [46]. A comparison of the cytokine transcripts that have been shown to be increased in response to an LPS challenge and attenuated by the absence of MK2 shows that many of those were not elevated 3- **(Supplementary Table 15)** or 5-days **(Supplementary Table 16)** post-MI. However, an important caveat to this comparison is that the time courses of the LPS studies are much shorter than 3-5 days. To examine the effects of MK2-deficiency more closely, the array data from MI-MK2$^{-/-}$ mice was normalized to the corresponding dataset from MI-MK2$^{+/+}$ mice (**Table 3**) and replotted as volcano plots **(Figure 10)**. Focusing on mRNAs that underwent a 2-fold change in abundance with $P < 0.05$, Figure 10 shows that at both 3- and 5-days post-MI, the absence of MK2 reduced the abundance of some mRNAs but increased the abundance of others. Furthermore, the effects of MK2-deficiency on transcript abundance differed both with respect to surviving versus infarcted myocardium and time post-MI. Three days post-MI, *Ifna2* was increased and *Il16* was decreased in infarcted MK2$^{-/-}$ tissue whereas in the non-infarcted myocardium *Il27* increased and *Tnfsf11*, *Ccl3*, and *Il1rn* decreased. Five days post-MI, *Ctf16* and *Il10* were increased in infarcted tissue whereas in the non-infarcted myocardium *Ccl9, Nodal, and Xcl2* increased and *Il15* decreased. Furthermore, as shown in Figure 9, in sham-operated mice 3 days post-surgery, *Il15* was reduced and *Il10* was increased in MK2-deficient hearts. Five-days post-surgery, *Il15* was decreased. These findings show that the absence of MK2 did modify the inflammatory response in the infarcted heart by both potentiating and attenuating the induction of various cytokines.

MK2-deficiency did not alter myofibroblast motility in vitro. HSP27/25, a small heat shock protein with actin-capping activity, is a substrate for MK2 [36, 44] and MK2-deficiency in immortalized MEFs, tracheal smooth muscle cells, endothelial cells, and macrophages decreases migration [77-79]. Since fibroblast recruitment is an important component of wound healing post-

MI, we next examined migration by scratch-wound assay in ventricular fibroblasts isolated from the hearts of $MK2^{+/+}$ and $MK2^{-/-}$ mice. Fibroblasts were grown to 80% confluence on a rigid plastic substrate, "wounds" were created, and the cells were incubated for an additional 24 h with or without the addition of serum alone or serum plus angiotensin II to the media. Wound areas were measured morphometrically at time 0 and after 24 h. The percentage of wound closure was comparable between genotypes under all 3 experimental conditions **(Figure 11)**. Hence, myofibroblast migration *in vitro* was not altered by the absence of MK2.

Discussion

MK2 plays a prominent role in the inflammatory response via both regulating the stability of many cytokine mRNAs and mediating the response of numerous cytokine receptors [80]. As inflammation is an important early phase of myocardial wound healing post-myocardial infarct, we examined the effects of MK2-deficiency in 3-month-old male mice 3- and 5-days after permanent ligation of the left anterior descending coronary artery (LAD). Mortality was reduced in MK2-deficient mice as the incidence of left ventricular (LV) wall rupture during the first 5 days of wound-healing post-MI was lower in MI-MK2$^{-/-}$ than MI-MK2$^{+/+}$ mice. However, MK2-deficiency did not affect infarct area or immune cell infiltration whereas LV dilation was attenuated in MI-MK2$^{-/-}$ mice. Hence, the MK2-deficiency did not impair the inflammatory phase of post-MI wound repair.

Wound healing post-MI progresses through three overlapping phases: inflammation, proliferation, and maturation [3, 5] and involves components of the innate immune system. Within the infarct, necrotic myocytes release damage-associated molecular patterns (DAMPs), resulting in the induction and release of pro-inflammatory cytokines and chemokines and the subsequent recruitment of neutrophils and monocytes. Monocytes differentiate into macrophages and, together, these cells phagocytose dead tissue and release inflammatory mediators. After several days, the inflammatory response begins to resolve. Appropriate induction and resolution of the inflammatory response is an important step prior to fibroblast activation, secretion of extracellular matrix proteins, and formation of a mature scar. MK2-deficiency can affect multiple aspects of the inflammatory response, including immune cell recruitment [47, 55, 81-83], macrophage activation [47, 84, 85], macrophage M1/M2 polarization [52, 74], cell motility [77, 81], cytokine/chemokine production [46, 47, 77, 81, 83, 85, 86], and signaling downstream of cytokine receptors [87-89]. The present study employed a global knockout model [77] to study the effects of an MK2-deficiency on the inflammatory phase of wound repair post-MI. This study examined mice on days 3 and 5 post-MI, as the primary cause of death in mice following LAD ligation is rupture of the LV wall at the infarct border on or around day 4 [63]. The area at risk and infarct area in MI-MK2$^{-/-}$ and MI-MK2$^{+/+}$

mice were similar. However, whereas fibroblast-targeted deletion of p38α, which, along with p38β, serves to activate MK2, resulted in 100% mortality following permanent LAD ligation [26], survival was actually increased in MK2-deficient mice five-days post-MI. Hence, the absence of MK2 activity was not detrimental overall to the inflammatory phase of wound-repair post-MI.

In response to pro-inflammatory mediators released by necrotic and apoptotic myocytes in the infarcted myocardium, circulating neutrophils and monocytes migrate to the infarct [20, 30] where they, along with resident fibroblasts, degrade the extracellular matrix, remove dead cells and debris, and participate in the inflammatory response by secreting numerous cytokines [27, 64, 68]. MK2 inhibition or deficiency has been shown to reduce myeloid cell recruitment [47, 55, 81-83], which likely results from the roles played by MK2 in cytokine/chemokine production, the cellular signaling downstream of cytokine/chemokine receptor activation, and cell motility. However, in the context of MI, MK2-deficiency did not alter the intensity of myeloperoxidase (MPO) immunostaining in the infarct or infarct border region, suggesting recruitment of neutrophils or monocytes was unaffected 3- or 5-days post-MI. This study would have missed changes in neutrophil recruitment, which peaks 1-day post-MI, and would not discriminate between Ly-6C^{hi} and Ly-6C^{lo} monocytes, which peak on day-3 and day-7 post-MI, respectively [30]. Ly-6C^{hi} monocytes are pro-inflammatory whereas Ly-6C^{lo} monocytes have been implicated in resolving the inflammatory response [30, 90-92]. In an inflammatory environment such as the infarct zone, monocytes differentiate into macrophages, supplementing the complement of resident macrophages [93, 94]. In the healthy myocardium, resident macrophages comprise both pro-inflammatory/M1 and anti-inflammatory/M2 phenotypes [94] where they phagocytose debris and apoptotic cells. Initially following MI, M1 macrophages predominate, contributing to acute inflammation and phagocytosis. As the inflammatory response progresses macrophages polarize towards the M2 phenotype, which are implicated in resolution of the inflammatory response and promote fibrosis. This polarization depends, in part, on the secretion of neutrophil gelatinase-associated lipocalin (NGAL) [95]. An MK2-deficiency does not affect the abundance of circulating

556 $CD14^+$ monocytes/macrophages [46], whereas macrophage recruitment and activation are reduced
557 [47, 77, 82, 85, 96]. In addition, in a mouse model of inflammation-driven colorectal cancer [75] and
558 compression-induced spinal cord injury [97], an MK2-deficiency reduces M2 polarization.
559 Similarly, IL4/IL-13-induced M2 polarization of human U-837 monocytic cell-derived
560 macrophages is reduced by the MK2 inhibitor PF 3644022 [75]. However, the abundance of M2
561 macrophages was not significantly reduced in the infarct or peri-infarct regions of MI-$MK2^{-/-}$
562 hearts post-MI. Although administration of MMI-0100, a cell-permeable peptide inhibitor of
563 MK2, was previously shown to improve systolic function post-MI [98, 99], in the present study,
564 systolic function in MI-$MK2^{-/-}$ mice did not differ significantly from MI-$MK2^{+/+}$ mice.
565 Furthermore, dilation was actually reduced in MI-$MK2^{-/-}$ hearts, which suggests the innate immune
566 response was unimpaired, and an excessive inflammatory response had not occurred.

567 The secretion of pro-inflammatory cytokines within the infarcted myocardium results in
568 fibroblast recruitment, proliferation, and activation to a myofibroblast phenotype (see [100]).
569 Myofibroblasts then secrete extracellular matrix proteins to create a scar and reinforce the damaged
570 ventricular wall. Although an MK2-deficiency impairs motility in mouse embryonic fibroblasts
571 [77], the motility of adult mouse ventricular myofibroblasts was not affected by the absence of MK2.
572 In addition, the abundance of myofibroblasts in the infarct or peri-infarct zone was not affected by
573 MK2-deficiency and, although early in the reparative process, only small differences were
574 observed in the collagen content within the infarct. Taken together, these observations suggest
575 that fibroblast activation was not affected by the absence of MK2 at least up until day 5 post-MI.
576 The effects of MK2-deficiency on the proliferative and maturation phases of wound repair post-
577 MI remain to be determined.

578 The coordinated production of pro- and anti-inflammatory cytokines orchestrates the onset
579 and resolution of the inflammatory phase of cardiac repair post-MI. Changes in cytokine mRNA,
580 assessed using pathway-targeted qPCR arrays (QIAGEN) and normalized to their respective sham
581 wild type levels, indicated that infarction resulted in an inflammatory response in both $MK2^{+/+}$ and

582 MK2$^{-/-}$ hearts. Indeed, the increased abundance of *Tgfb*2 mRNA, an anti-inflammatory cytokine,
583 as well as the decreased abundance of transcripts for *Bmp7*, a *Tgfb2* antagonist, and *Il15*, a pro-
584 inflammatory cytokine, were observed in infarcted MK2$^{+/+}$ and MK2$^{-/-}$ tissue 3 days post-MI [101-
585 107]. In addition, the abundance of *Il11* mRNA, a cytokine secreted by fibroblasts in response to
586 TGF-β, was also increased in infarcts of both genotypes [108, 109]. A decreased abundance of *Il15*
587 mRNA is also detected in all tissues 5 days post-MI. Previous studies observed that the absence
588 of MK2 reduces the abundance of mRNA for numerous cytokines when an inflammatory response
589 is evoked [46]. Normalizing qPCR array data from MK2-deficient tissue to the corresponding wild
590 type tissue revealed that, 3-days post-MI, the abundance of *Ifna2* mRNA was increased and *Il16*
591 was decreased in infarcted tissue whereas in the non-infarcted myocardium *Il27* increased and
592 *Tnfsf11*, *Ccl3*, and *Il1rn* were decreased in MK2-deficient tissue relative to wild type. Five days
593 post-MI, the abundance of *Ctf16* and *Il10* increased in MK2-deficient infarcted tissue whereas in
594 the non-infarcted myocardium *Ccl9, Nodal, and Xcl2* increased and *Il15* decreased. Hence, during
595 the inflammatory phase of wound repair following MI, the absence of MK2 resulted in both
596 increases and decreases in cytokine mRNA.

597

598 ***Conclusions***. In conclusion, the present study shows that, although the mRNA levels for several
599 cytokines were affected, an MK2-deficiency did not impair the inflammatory phase of wound
600 healing following myocardial infarction. In fact, rather than increased mortality, mice deficient in
601 MK2 showed reduced dilation and a significantly higher survival rate than wild type mice. It
602 remains to be determined if a deficiency in MK2 is detrimental to collagen deposition or scar
603 maturation.

Additional information

Competing interest

The authors declare no competing interest.

Author contributions

JT, SAN, PS, MGS, and BGA conceived and designed the experiments. JT, SAN, PS, FS, ND, DG, MAG, YS, CT, and MECL performed the experiments and analyzed the data. JT and BGA assembled and interpreted all the data. MG provided the mouse model. JT and BGA wrote and critically reviewed the manuscript. All authors have approved the final version of the current manuscript.

Funding

This work is supported by grants from the Heart and Stroke Foundation of Canada (Grant Numbers G-14-0006060 and G-18-0022227), and the Montreal Heart Institute Foundation to BGA. JCT holds the Canada Research Chair in translational and personalized medicine and the Université de Montréal Pfizer endowed research chair in atherosclerosis.

Acknowledgements

We thank Ms. Karine Nadeau for animal care and breeding.

Figure Legends

Figure 1. MK2-deficiency improved post-MI survival during the inflammatory phase and did not alter area at risk or infarct size. **A**, Kaplan-Meier survival curve for $MK2^{+/+}$ (solid line, n = 45) and $MK2^{-/-}$ (dashed line, n = 41) mice in the first 3 days post-MI. **B**, Kaplan-Meier survival curve for $MK2^{+/+}$ (solid line, n = 29) and $MK2^{-/-}$ (dashed line, n = 21) mice in the first 5 days post-MI (*, Mandel-Cox test: $P = 0.0285$). **C**, Area at risk (AAR) was assessed by infusion of Evans blue dye in $MK2^{+/+}$ (n = 6) and $MK2^{-/-}$ mice (n = 9) 30 minutes after ligation of the left anterior descending coronary artery. The AAR, which corresponds to the area in which the dye was excluded, is expressed as a percentage of the left ventricular (LV) wall area. **D**, Infarct area (IA) was assessed by 2,3,5-triphenyl tetrazolium chloride (TTC) staining in $MK2^{+/+}$ (n = 6) and $MK2^{-/-}$ mice (n = 9). Non-viable myocardium, which is not stained by TTC, is expressed as a percentage of the AAR. The number of animals in each group is indicated in parentheses. Shapiro-Wilk tests for normality were performed on all data. Results shown are median (first quartile and third quartile). Mann-Whitney tests were performed for statistical comparisons.

Figure 2. MK2-deficiency attenuated LV dilation five days post-MI. **A**, Basal lateral systolic contractile velocity (S_L). **B**, Basal septal systolic contractile velocity (S_S). **C**, Left ventricular (LV) dimension at end cardiac diastole (LVD_d). **D**, LV diameter at end cardiac systole (LVD_s). **E**, LV volume at end cardiac diastole (LVV_d). **F**, LV volume at end cardiac systole (LVV_s). Sham-$MK2^{+/+}$ (solid black circles, 3 days n = 17, 5 days n = 20), sham-$MK2^{-/-}$ (open blue circles, 3 days n = 18 - 19, 5 days n = 17), MI-$MK2^{+/+}$ (solid black squares, 3 days n = 15 - 16, 5 days n = 20 - 23) and MI-$MK2^{-/-}$ (open blue squares, 3 days n = 20, 5 days n = 19) mice. Data are presented as median (first quartile and third quartile). Shapiro-Wilk tests for normality were performed on all data. Data with a lognormal distribution were log-transformed prior to statistical comparison by two-way ANOVA, which included a factor for surgery (sham, LADL), a factor for genotype ($MK2^{+/+}$, $MK2^{-/-}$), and a surgery x genotype interaction term. The ANOVA was followed by Tukey's post hoc tests for multiple comparisons. $*P < 0.05$, $**P < 0.01$, $***P < 0.001$,

646 ****$P < 0.0001$.

647 **Figure 3. MK2-deficiency did not alter infarct area 3- or 5-days post-MI.** **A**, Representative
648 images of a hearts cut along the short axis (1). Sections taken from the upper region of the infarct
649 are identified as "Section A" and those from the lower region as "Section B" (2, 3). Sections from
650 both regions were employed for histological (Masson's trichrome stain) or immunohistochemical
651 stain (4). **B**, Representative Masson's trichrome stained short-axis sections of the ventricular
652 myocardium from sham and ligated $MK2^{+/+}$ and $MK2^{-/-}$ mice 5 days post-myocardial infarction
653 (MI) showing collagen deposition (blue) and healthy tissue (red). **C**, Infarct area, identified by
654 Masson's trichrome staining, expressed as a percentage of the total myocardial area from $MK2^{+/+}$
655 (solid black circles: Section A, n = 8; solid black squares: Section B, n = 6 - 8) and $MK2^{-/-}$ (open
656 blue circles: Section A, n = 6 - 7; open blue squares: Section B, n = 6 - 7) mice. Data are presented
657 as median (first quartile and third quartile). Shapiro-Wilk tests for normality were performed on
658 all data. Mann-Whitney tests were performed for statistical comparisons between $MK2^{+/+}$ and
659 $MK2^{-/-}$.

660 **Figure 4. MK2-deficiency did not hinder collagen deposition 3- and 5-days post-MI.** **A**,
661 Masson's trichrome stained short-axis sections of the ventricular myocardium from $MK2^{+/+}$ and
662 $MK2^{-/-}$ mice 3- and 5-days post-myocardial infarction (MI) showing collagen deposition (blue)
663 and healthy tissue (red). Hearts were cut along the short axis through the center of the infarct to
664 yield upper (Section A) and lower, (Section B) regions. **B**, Collagen content expressed as a
665 percentage of the total infarct area from $MK2^{+/+}$ (solid black circles: Section A, n = 8; solid black
666 squares: Section B, n = 7 and 8) and $MK2^{-/-}$ (open blue circles: Section A, n = 7 - 8; open blue
667 squares: Section B, n = 7 - 8) mice. Images were analyzed by color segmentation using Image Pro
668 Plus version 7.0 (Media Cybernetics, Silver Spring, MD). Shapiro-Wilk tests for normality were
669 performed on all data. Data are presented as median (first quartile and third quartile). Mann-
670 Whitney tests were performed for statistical comparisons between $MK2^{+/+}$ and $MK2^{-/-}$. *$P < 0.05$.

Figure 5. MK2-deficiency did not hinder recruitment of neutrophils and monocytes to the peri-infarct and infarct areas 3- and 5-days post-MI. **A**. Representative images of immunohistochemical staining for myeloperoxidase (MPO, dark brown), a neutrophil and monocyte marker, in sham and infarcted hearts from $MK2^{+/+}$ and $MK2^{-/-}$ mice euthanized 3- and 5-days post-MI. Hearts were cut along the short axis through the center of the infarct to yield upper (Section A) and lower, (Section B) regions. **B**, MPO immunoreactivity expressed as a percentage of the total field area from sham-$MK2^{+/+}$ (black circles, n = 4 - 7), MI-$MK2^{+/+}$ (non-infarcted tissue: black squares, n = 6 - 8; peri-infarct: black triangles, n = 5 - 7; infarct: inverted black triangles, n = 5 - 7), sham-$MK2^{-/-}$ (blue circles, n = 4 - 8), and MI-$MK2^{-/-}$ (non-infarcted tissue: blue squares, n = 6 - 8; peri-infarct: blue triangles, n = 6 - 8; infarct: inverted blue triangles, n = 3 - 8) hearts. Images were analyzed by color segmentation using Image Pro Plus version 7.0 (Media Cybernetics, Silver Spring, MD). Shapiro-Wilk tests for normality were performed on all data. Data are presented as median (first quartile and third quartile). Data with a lognormal distribution were log-transformed prior to statistical comparison by two-way ANOVA, which included a factor for surgery (sham, MI), a factor for genotype ($MK2^{+/+}$, $MK2^{-/-}$), and a surgery x genotype interaction term. No interaction was detected ($P > 0.05$). The ANOVA was followed by Tukey's post hoc tests for multiple comparisons. $^{*}P < 0.05$, $^{**}P < 0.01$, $^{***}P < 0.001$, $^{****}P < 0.0001$.

Figure 6. MK2-deficiency did not hinder M2 macrophage recruitment to the peri-infarct area 3- and 5-days post-MI. **A**, Representative images of immunohistochemical staining of the mannose receptor cluster of differentiation 206 (CD206, dark brown), an M2 macrophage marker, in sham and infarcted hearts from $MK2^{+/+}$ and $MK2^{-/-}$ mice sacrificed 3- and 5-days post-MI. Hearts were cut along the short axis through the center of the infarct to yield two pieces (Section A, upper region; Section B, lower region). **B**, CD206 immunostaining expressed as a percentage of the total field area from sham-$MK2^{+/+}$ (black circles, n = 7 - 8), MI-$MK2^{+/+}$ (non-infarcted tissue: black squares, n = 7 - 8; peri-infarct: black triangles, n = 7 - 8; infarct: black inverted triangles, n = 6

- 8), sham-MK2$^{-/-}$ (blue circles, n= 8), and MI-MK2$^{-/-}$ (non-infarcted tissue: blue squares, n = 5 - 8; peri-infarct: blue triangles, n = 5 - 8; infarct: blue inverted triangles, n = 6 - 8) hearts. Images were analyzed by color segmentation using Image Pro Plus version 7.0 (Media Cybernetics, Silver Spring, MD). Shapiro-Wilk tests for normality were performed on all data. Data are presented as median (first quartile and third quartile). Data with a lognormal distribution were log-transformed prior to statistical comparison by two-way ANOVA, which included a factor for surgery (sham, MI), a factor for genotype (MK2$^{+/+}$, MK2$^{-/-}$), and a surgery x genotype interaction term. No interaction was detected ($P > 0.05$). The ANOVA was followed by Tukey's post hoc tests for multiple comparisons. *$P < 0.05$, **$P < 0.01$, ***$P < 0.001$, ****$P < 0.0001$.

Figure 7. MK2-deficiency did not alter the distribution or abundance of myofibroblasts 3- and 5-days post-MI. A: Representative images of immunohistochemical staining of smooth muscle alpha-actin (α-SMA, dark brown), a myofibroblast marker, in sham and infarcted hearts from MK2$^{+/+}$ and MK2$^{-/-}$ mice sacrificed 3- and 5-days post-MI. Hearts were cut along the short axis through the center of the infarct to yield two pieces (Section A, upper region; Section B, lower region). **B**, α-SMA immunostaining expressed as a percentage of the total field area from sham-MK2$^{+/+}$ (black circles, n = 7 - 8), MI-MK2$^{+/+}$ (non-infarcted tissue: black squares, n = 7 - 8; peri-infarct: black triangles, n = 7 - 8; infarct: black inverted triangles, n = 6 - 8), sham-MK2$^{-/-}$ (blue circles, n = 8), and MI-MK2$^{-/-}$ (non-infarcted tissue: blue squares, n = 5 - 8; peri-infarct: blue triangles, n = 5 - 8; infarct: blue inverted triangles, n = 5 - 8) hearts. Images were analyzed by color segmentation using Image Pro Plus version 7.0 (Media Cybernetics, Silver Spring, MD). Shapiro-Wilk tests for normality were performed on all data. Data are presented as median (first quartile and third quartile). Data with a lognormal distribution were log-transformed prior to statistical comparison by two-way ANOVA, which included a factor for surgery (sham, MI), a factor for genotype (MK2$^{+/+}$, MK2$^{-/-}$), and a surgery x genotype interaction term. No interaction was detected ($P > 0.05$). The ANOVA was followed by Tukey's post hoc tests for multiple comparisons. *$P < 0.05$, **$P < 0.01$, ***$P < 0.001$, ****$P < 0.0001$.

Figure 8. MK2-deficient hearts showed a greater increase in endothelial cell abundance in their peri-infarct region 5 days post-MI. **A**, Representative images of immunohistochemical staining of the cluster of differentiation 31 protein (CD31, dark brown), an endothelial cell marker, in $MK2^{+/+}$ and $MK2^{-/-}$ sham and infarct hearts collected 3- and 5-days post-MI. Hearts were cut along the short axis through the center of the infarct to yield two pieces (Section A, upper region; Section B, lower region). **B**, CD31 immunostaining expressed as a percentage of the total field area from sham-$MK2^{+/+}$ (black circles, n = 4 - 8) and MI-$MK2^{+/+}$ (non-infarcted tissue: black squares, n = 5 - 8; peri-infarct: black triangles, n = 5 - 7; infarct: black inverted triangles, n = 4 - 7), sham-$MK2^{-/-}$ (blue circles, n = 4 - 8), and MI-$MK2^{-/-}$ (non-infarcted tissue: blue squares, n = 3 - 8; peri-infarct: blue triangles, n = 5 - 8; infarct: blue inverted triangles, n = 4 - 8) hearts. Images were analyzed by color segmentation using Image Pro Plus version 7.0 (Media Cybernetics, Silver Spring, MD). Shapiro-Wilk tests for normality were performed on all data. Data are presented as median (first quartile and third quartile). Data with a lognormal distribution were log-transformed prior to statistical comparison by two-way ANOVA, which included a factor for surgery (sham, MI), a factor for genotype ($MK2^{+/+}$, $MK2^{-/-}$), and a surgery x genotype interaction term. A significant surgery x genotype interaction ($P < 0.05$) was detected in the 'B' sections 5-days post-MI. The ANOVA was followed by Tukey's post hoc tests for multiple comparisons. $*P < 0.05$, $**P < 0.01$, $***P < 0.001$, $****P < 0.0001$. **C**, Density of new vessels as determined by the number of CD31-positive capillaries that are 20 μm in diameter or less per mm^2 found in the peri-infarct region of $MK2^{+/+}$ (n = 5 - 7) and $MK2^{-/-}$ (n = 7) hearts. Data are presented as median (first quartile and third quartile). Mann-Whitney tests were performed for statistical comparisons between $MK2^{+/+}$ and $MK2^{-/-}$. $*P < 0.05$.

Figure 9. MK2-deficiency alters transcript expression pattern but does not impair overall inflammatory response. Volcano plots showing the abundance of inflammatory transcripts in sham, healthy and infarct left ventricular (LV) tissue from $MK2^{+/+}$ and $MK2^{-/-}$ mice 3- and 5-days post-MI (n = 3 to 4). mRNA abundance was quantified using RT^2 Profiler PCR Arrays (QIAGEN

749 PAMM-150Z). Each transcript was normalized to its abundance in sham-MK2$^{+/+}$ LV tissues (n =
750 3 - 4) at day 3 or day 5 post-MI. Some transcripts that underwent significant changes have been
751 labeled. Transcripts above the horizontal dotted line showed a fold change with $P < 0.05$.
752 Transcripts found outside of the vertical dotted lines underwent a 2-fold change in abundance (left,
753 decreased abundance; right, increased abundance).

754 **Figure 10. MK2-deficiency leads to a different pro- and anti-inflammatory signature in both**
755 **infract and healthy tissues at 3- and 5-days post-MI.** Volcano plots representing the abundance
756 of inflammatory transcripts in MK2-deficient infarct or healthy tissues normalized to the
757 corresponding MK2$^{+/+}$ heart tissue (n = 3 to 4). mRNA abundance was quantified using RT^2
758 Profiler PCR Arrays (QIAGEN PAMM-150Z). Transcripts that underwent a significant change
759 are labeled. Transcripts above the horizontal dotted line showed a fold change with $P < 0.05$.
760 Transcripts found outside of the vertical dotted lines underwent a 2-fold change in abundance (left,
761 decreased abundance; right, increased abundance).

762 **Figure 11. MK2-deficiency does not alter myofibroblast motility *in vitro*.** **A**, Representative
763 images of scratch wound assays of left ventricular myocardial myofibroblasts isolated from
764 MK2$^{+/+}$ and MK2$^{-/-}$ mice. Scratches were imposed once cell confluency reached 80%. Cells were
765 then incubated for 24 h with serum-free media (control), media supplemented with 10% serum, or
766 media supplemented with 10% serum and angiotensin II (Ang II, 1 μM). Open wound area (space
767 between vertical dotted lines) was measured at times 0 and 24 h and wound closure was calculated.
768 **B**, Motility, expressed as percentage of wound area remaining open after 24 h. Data was
769 normalized to the values for MK2$^{+/+}$ myofibroblasts maintained in serum-free media (6.26 ±
770 16.5%) and are presented as mean ± SEM (n = 4). MK2$^{+/+}$, solid bars; MK2$^{+/+}$, open bars.
771 Statistical analysis was done by 2-way ANOVA followed by Tukey's post hoc test.

772 **References:**

773

774

775 1. Thygesen K, Alpert JS, Jaffe AS, Simoons ML, Chaitman BR, White HD, Writing Group
776 on behalf of the Joint ESCAAHAWHFTFftUDoMI. Third universal definition of
777 myocardial infarction. *Glob Heart*. 2012;7:275-295

778 2. Saleh M, Ambrose JA. Understanding myocardial infarction. *F1000Res*. 2018;7

779 3. Shinde AV, Frangogiannis NG. Fibroblasts in myocardial infarction: a role in
780 inflammation and repair. *J Mol Cell Cardiol*. 2014;70:74-82

781 4. Cleutjens JP, Blankesteijn WM, Daemen MJ, Smits JF. The infarcted myocardium: simply
782 dead tissue, or a lively target for therapeutic interventions. *Cardiovasc Res*. 1999;44:232-
783 241

784 5. Frangogiannis NG. Chemokines in ischemia and reperfusion. *Thromb Haemost*.
785 2007;97:738-747

786 6. Leonard WJ. *Cytokines: From Basic Mechanisms of Cellular Control to New Therapeutics*.
787 New York: Cold Spring Harbor Laboratory Press; 2018.

788 7. Nah DY, Rhee MY. The inflammatory response and cardiac repair after myocardial
789 infarction. *Korean Circ J*. 2009;39:393-398

790 8. Stieger P, Daniel JM, Tholen C, Dutzmann J, Knopp K, Gunduz D, Aslam M,
791 Kampschulte M, Langheinrich A, Fischer S*, et al.* Targeting of Extracellular RNA Reduces

Edema Formation and Infarct Size and Improves Survival After Myocardial Infarction in Mice. *J Am Heart Assoc*. 2017;6:e004541

9. Dinarello CA. Overview of the IL-1 family in innate inflammation and acquired immunity. *Immunol Rev*. 2018;281:8-27

10. Sager HB, Kessler T, Schunkert H. Monocytes and macrophages in cardiac injury and repair. *J Thorac Dis*. 2017;9:S30-S35

11. Ma Y, Iyer RP, Jung M, Czubryt MP, Lindsey ML. Cardiac Fibroblast Activation Post-Myocardial Infarction: Current Knowledge Gaps. *Trends Pharmacol Sci*. 2017;38:448-458

12. Pagel CN, Wasgewatte Wijesinghe DK, Taghavi Esfandouni N, Mackie EJ. Osteopontin, inflammation and myogenesis: influencing regeneration, fibrosis and size of skeletal muscle. *J Cell Commun Signal*. 2014;8:95-103

13. Pare A, Mailhot B, Levesque SA, Juzwik C, Ignatius Arokia Doss PM, Lecuyer MA, Prat A, Rangachari M, Fournier A, Lacroix S. IL-1β enables CNS access to CCR2^{hi} monocytes and the generation of pathogenic cells through GM-CSF released by CNS endothelial cells. *Proc Natl Acad Sci U S A*. 2018;115:E1194-E1203

14. Shi C, Pamer EG. Monocyte recruitment during infection and inflammation. *Nat Rev Immunol*. 2011;11:762-774

15. Soehnlein O, Lindbom L, Weber C. Mechanisms underlying neutrophil-mediated monocyte recruitment. *Blood*. 2009;114:4613-4623

16. Tian M, Yuan YC, Li JY, Gionfriddo MR, Huang RC. Tumor necrosis factor-α and its role as a mediator in myocardial infarction: A brief review. *Chronic Dis Transl Med*. 2015;1:18-26

17. Gerdes N, Sukhova GK, Libby P, Reynolds RS, Young JL, Schonbeck U. Expression of interleukin (IL)-18 and functional IL-18 receptor on human vascular endothelial cells, smooth muscle cells, and macrophages: implications for atherogenesis. *J Exp Med*. 2002;195:245-257

18. Mouton AJ, DeLeon-Pennell KY, Rivera Gonzalez OJ, Flynn ER, Freeman TC, Saucerman JJ, Garrett MR, Ma Y, Harmancey R, Lindsey ML. Mapping macrophage polarization over the myocardial infarction time continuum. *Basic Res Cardiol*. 2018;113:26

19. Takawale A, Zhang P, Azad A, Wang W, Wang X, Murray AG, Kassiri Z. Myocardial overexpression of TIMP3 following myocardial infarction exerts beneficial effects through promoting angiogenesis and suppressing early proteolysis. *Am J Physiol Heart Circ Physiol*. 2017:ajpheart 00108 02017

20. Ng LG, Ostuni R, Hidalgo A. Heterogeneity of neutrophils. *Nat Rev Immunol*. 2019;19:255-265

21. Maher JF, Mallory GK, Laurenz GA. Rupture of the heart after myocardial infarction. *N Engl J Med*. 1956;255:1-10

22. Gao XM, Ming Z, Su Y, Fang L, Kiriazis H, Xu Q, Dart AM, Du XJ. Infarct size and post-infarct inflammation determine the risk of cardiac rupture in mice. *Int J Cardiol*. 2010;143:20-28

832 23. Travers JG, Kamal FA, Robbins J, Yutzey KE, Blaxall BC. Cardiac Fibrosis: The
833 Fibroblast Awakens. *Circ Res*. 2016;118:1021-1040

834 24. Ivey MJ, Kuwabara JT, Pai JT, Moore RE, Sun Z, Tallquist MD. Resident fibroblast
835 expansion during cardiac growth and remodeling. *J Mol Cell Cardiol*. 2018;114:161-174

836 25. Mishra PK, Pathi V, Murday A. Post myocardial infarction left ventricular free wall
837 rupture. *Interact Cardiovasc Thorac Surg*. 2007;6:39-42

838 26. Molkentin JD, Bugg D, Ghearing N, Dorn LE, Kim P, Sargent MA, Gunaje J, Otsu K,
839 Davis J. Fibroblast-Specific Genetic Manipulation of p38 Mitogen-Activated Protein
840 Kinase In Vivo Reveals Its Central Regulatory Role in Fibrosis. *Circulation*.
841 2017;136:549-561

842 27. Lech M, Anders HJ. Macrophages and fibrosis: How resident and infiltrating mononuclear
843 phagocytes orchestrate all phases of tissue injury and repair. *Biochim Biophys Acta*.
844 2013;1832:989-997

845 28. Collier P, Watson CJ, van Es MH, Phelan D, McGorrian C, Tolan M, Ledwidge MT,
846 McDonald KM, Baugh JA. Getting to the heart of cardiac remodeling; how collagen
847 subtypes may contribute to phenotype. *J Mol Cell Cardiol*. 2012;52:148-153

848 29. Horn MA, Trafford AW. Aging and the cardiac collagen matrix: Novel mediators of
849 fibrotic remodelling. *J Mol Cell Cardiol*. 2016;93:175-185

30. Nahrendorf M, Swirski FK, Aikawa E, Stangenberg L, Wurdinger T, Figueiredo JL, Libby P, Weissleder R, Pittet MJ. The healing myocardium sequentially mobilizes two monocyte subsets with divergent and complementary functions. *J Exp Med*. 2007;204:3037-3047

31. Korns D, Frasch SC, Fernandez-Boyanapalli R, Henson PM, Bratton DL. Modulation of macrophage efferocytosis in inflammation. *Front Immunol*. 2011;2:57

32. Elliott MR, Koster KM, Murphy PS. Efferocytosis Signaling in the Regulation of Macrophage Inflammatory Responses. *J Immunol*. 2017;198:1387-1394

33. Ma Y, Mouton AJ, Lindsey ML. Cardiac macrophage biology in the steady-state heart, the aging heart, and following myocardial infarction. *Transl Res*. 2018;191:15-28

34. Risco A, Cuenda A. New Insights into the p38γ and p38δ MAPK Pathways. *J Signal Transduct*. 2012;2012:520289

35. Cross HR, Li M, Petrich BG, Murphy E, Wang Y, Steenbergen C. Effect of p38 MAP kinases on contractility and ischemic injury in intact heart. *Acta Physiol Hung*. 2009;96:307-323

36. Fiore M, Forli S, Manetti F. Targeting Mitogen-Activated Protein Kinase-Activated Protein Kinase 2 (MAPKAPK2, MK2): Medicinal Chemistry Efforts To Lead Small Molecule Inhibitors to Clinical Trials. *J Med Chem*. 2016;59:3609-3634

37. Menon MB, Gropengiesser J, Fischer J, Novikova L, Deuretzbacher A, Lafera J, Schimmeck H, Czymmeck N, Ronkina N, Kotlyarov A*, et al.* p38^{MAPK}/MK2-dependent

phosphorylation controls cytotoxic RIPK1 signalling in inflammation and infection. *Nat Cell Biol*. 2017;19:1248-1259

38. Kim EK, Choi EJ. Pathological roles of MAPK signaling pathways in human diseases. *Biochim Biophys Acta*. 2010;1802:396-405

39. Dingar D, Benoit MJ, Mamarbachi AM, Villeneuve LR, Gillis MA, Grandy S, Gaestel M, Fiset C, Allen BG. Characterization of the expression and regulation of MK5 in the murine ventricular myocardium. *Cell Signal*. 2010;22:1063-1075

40. Moens U, Kostenko S, Sveinbjornsson B. The Role of Mitogen-Activated Protein Kinase-Activated Protein Kinases (MAPKAPKs) in Inflammation. *Genes (Basel)*. 2013;4:101-133

41. Coulombe P, Meloche S. Atypical mitogen-activated protein kinases: structure, regulation and functions. *Biochim Biophys Acta*. 2007;1773:1376-1387

42. Arthur JS, Ley SC. Mitogen-activated protein kinases in innate immunity. *Nat Rev Immunol*. 2013;13:679-692

43. Soni S, Anand P, Padwad YS. MAPKAPK2: the master regulator of RNA-binding proteins modulates transcript stability and tumor progression. *J Exp Clin Cancer Res*. 2019;38:121

44. Gurgis FM, Ziaziaris W, Munoz L. Mitogen-activated protein kinase-activated protein kinase 2 in neuroinflammation, heat shock protein 27 phosphorylation, and cell cycle: role and targeting. *Mol Pharmacol*. 2014;85:345-356

45. Tanaka T, Iino M, Goto K. Sec6 enhances cell migration and suppresses apoptosis by elevating the phosphorylation of p38 MAPK, MK2, and HSP27. *Cell Signal*. 2018;49:1-16

889 46. Kotlyarov A, Neininger A, Schubert C, Eckert R, Birchmeier C, Volk HD, Gaestel M.
890 MAPKAP kinase 2 is essential for LPS-induced TNF-α biosynthesis. *Nat Cell Biol*.
891 1999;1:94-97

892 47. Phinney BB, Ray AL, Peretti AS, Jerman SJ, Grim C, Pinchuk IV, Beswick EJ. MK2
893 Regulates Macrophage Chemokine Activity and Recruitment to Promote Colon Tumor
894 Growth. *Front Immunol*. 2018;9:1857

895 48. Menon MB, Gaestel M. MK2-TNF-Signaling Comes Full Circle. *Trends Biochem Sci*.
896 2017

897 49. Khabar KS. Hallmarks of cancer and AU-rich elements. *WIREs RNA*. 2017;8:e1368

898 50. Singh RK, Najmi AK, Dastidar SG. Biological functions and role of mitogen-activated
899 protein kinase activated protein kinase 2 (MK2) in inflammatory diseases. *Pharmacol Rep*.
900 2017;69:746-756

901 51. Gaestel M. What goes up must come down: molecular basis of MAPKAP kinase 2/3-
902 dependent regulation of the inflammatory response and its inhibition. *Biol Chem*.
903 2013;394:1301-1315

904 52. de Boer JF, Dikkers A, Jurdzinski A, von Felden J, Gaestel M, Bavendiek U, Tietge UJ.
905 Mitogen-activated protein kinase-activated protein kinase 2 deficiency reduces insulin
906 sensitivity in high-fat diet-fed mice. *PLoS One*. 2014;9:e106300

907 53. Streicher JM, Ren S, Herschman H, Wang Y. MAPK-activated protein kinase-2 in cardiac
908 hypertrophy and cyclooxygenase-2 regulation in heart. *Circ Res*. 2010;106:1434-1443

909 54. Hegen M, Gaestel M, Nickerson-Nutter CL, Lin LL, Telliez JB. MAPKAP kinase 2-
910 deficient mice are resistant to collagen-induced arthritis. *J Immunol*. 2006;177:1913-1917

911 55. Jagavelu K, Tietge UJ, Gaestel M, Drexler H, Schieffer B, Bavendiek U. Systemic
912 deficiency of the MAP kinase-activated protein kinase 2 reduces atherosclerosis in
913 hypercholesterolemic mice. *Circ Res*. 2007;101:1104-1112

914 56. Ruiz M, Coderre L, Lachance D, Houde V, Martel C, Thompson Legault J, Gillis MA,
915 Bouchard B, Daneault C, Carpentier AC*, et al.* MK2 Deletion in Mice Prevents Diabetes-
916 Induced Perturbations in Lipid Metabolism and Cardiac Dysfunction. *Diabetes*.
917 2016;65:381-392

918 57. Ozcan L, Xu X, Deng SX, Ghorpade DS, Thomas T, Cremers S, Hubbard B, Serrano-Wu
919 MH, Gaestel M, Landry DW*, et al.* Treatment of Obese Insulin-Resistant Mice With an
920 Allosteric MAPKAPK2/3 Inhibitor Lowers Blood Glucose and Improves Insulin
921 Sensitivity. *Diabetes*. 2015;64:3396-3405

922 58. Singh RK, Diwan M, Dastidar SG, Najmi AK. Differential effect of p38 and MK2 kinase
923 inhibitors on the inflammatory and toxicity biomarkers in vitro. *Hum Exp Toxicol*.
924 2018;37:521-531

925 59. Shi P, Zhang L, Zhang M, Yang W, Wang K, Zhang J, Otsu K, Huang G, Fan X, Liu J.
926 Platelet-Specific p38α Deficiency Improved Cardiac Function After Myocardial Infarction
927 in Mice. *Arterioscler Thromb Vasc Biol*. 2017;37:e185-e196

928 60. Ruiz M, Khairallah M, Dingar D, Vaniotis G, Khairallah RJ, Lauzier B, Thibault S,
929 Trépanier J, Shi Y, Douillette A*, et al.* MK2-deficient mice are bradycardic and display

delayed hypertrophic remodelling in response to a chronic increase in afterload. *J. Am. Heart Assoc.* 2020

61. Ruiz M, Coderre L, Allen BG, Rosiers CD. Protecting the heart through MK2 modulation, toward a role in diabetic cardiomyopathy and lipid metabolism. *Biochim Biophys Acta*. 2017

62. Dingar D, Merlen C, Grandy S, Gillis MA, Villeneuve LR, Mamarbachi AM, Fiset C, Allen BG. Effect of pressure overload-induced hypertrophy on the expression and localization of p38 MAP kinase isoforms in the mouse heart. *Cell Signal*. 2010;22:1634-1644

63. Nawaito SA, Sahadevan P, Clavet-Lanthier ME, Pouliot P, Sahmi F, Shi Y, Gillis MA, Lesage F, Gaestel M, Sirois MG*, et al.* MK5 haplodeficiency decreases collagen deposition and scar size during post-myocardial infarction wound repair. *Am J Physiol Heart Circ Physiol*. 2019;316:H1281-H1296

64. Nawaito SA, Dingar D, Sahadevan P, Hussein B, Sahmi F, Shi Y, Gillis MA, Gaestel M, Tardif JC, Allen BG. MK5 haplodeficiency attenuates hypertrophy and preserves diastolic function during remodeling induced by chronic pressure overload in the mouse heart. *Am J Physiol Heart Circ Physiol*. 2017;313:H46-H58

65. Liao Y, Ishikura F, Beppu S, Asakura M, Takashima S, Asanuma H, Sanada S, Kim J, Ogita H, Kuzuya T*, et al.* Echocardiographic assessment of LV hypertrophy and function in aortic-banded mice: necropsy validation. *Am J Physiol Heart Circ Physiol*. 2002;282:H1703-1708

951 66. Nawaito SA, Sahadevan P, Sahmi F, Gaestel M, Calderone A, Allen BG. Transcript levels
952 for extracellular matrix proteins are altered in MK5-deficient cardiac ventricular
953 fibroblasts. *J Mol Cell Cardiol*. 2019;132:164-177

954 67. Kendall RW, DeWood MA. Postinfarction cardiac rupture: surgical success and review of
955 the literature. *Ann Thorac Surg*. 1978;25:311-315

956 68. Varol C, Mildner A, Jung S. Macrophages: development and tissue specialization. *Annu*
957 *Rev Immunol*. 2015;33:643-675

958 69. Humeres C, Vivar R, Boza P, Munoz C, Bolivar S, Anfossi R, Osorio JM, Olivares-Silva
959 F, Garcia L, Diaz-Araya G. Cardiac fibroblast cytokine profiles induced by
960 proinflammatory or profibrotic stimuli promote monocyte recruitment and modulate
961 macrophage M1/M2 balance in vitro. *J Mol Cell Cardiol*. 2016

962 70. Segers VFM, Brutsaert DL, De Keulenaer GW. Cardiac Remodeling: Endothelial Cells
963 Have More to Say Than Just NO. *Front Physiol*. 2018;9:382

964 71. Hendrickx J, Doggen K, Weinberg EO, Van Tongelen P, Fransen P, De Keulenaer GW.
965 Molecular diversity of cardiac endothelial cells in vitro and in vivo. *Physiol Genomics*.
966 2004;19:198-206

967 72. Favero G, Paganelli C, Buffoli B, Rodella LF, Rezzani R. Endothelium and its alterations
968 in cardiovascular diseases: life style intervention. *Biomed Res Int*. 2014;2014:801896

969 73. Thuraisingam T, Xu YZ, Eadie K, Heravi M, Guiot MC, Greemberg R, Gaestel M,
970 Radzioch D. MAPKAPK-2 signaling is critical for cutaneous wound healing. *J Invest*
971 *Dermatol*. 2010;130:278-286

972 74. Suarez-Lopez L, Kong YW, Sriram G, Patterson JC, Rosenberg S, Morandell S, Haigis
973 KM, Yaffe MB. MAPKAP Kinase-2 Drives Expression of Angiogenic Factors by Tumor-
974 Associated Macrophages in a Model of Inflammation-Induced Colon Cancer. *Front*
975 *Immunol*. 2020;11:607891

976 75. Suarez-Lopez L, Sriram G, Kong YW, Morandell S, Merrick KA, Hernandez Y, Haigis
977 KM, Yaffe MB. MK2 contributes to tumor progression by promoting M2 macrophage
978 polarization and tumor angiogenesis. *Proc Natl Acad Sci U S A*. 2018;115:E4236-E4244

979 76. DeLisser HM, Christofidou-Solomidou M, Strieter RM, Burdick MD, Robinson CS,
980 Wexler RS, Kerr JS, Garlanda C, Merwin JR, Madri JA*, et al.* Involvement of endothelial
981 PECAM-1/CD31 in angiogenesis. *Am J Pathol*. 1997;151:671-677

982 77. Kotlyarov A, Yannoni Y, Fritz S, Laass K, Telliez JB, Pitman D, Lin LL, Gaestel M.
983 Distinct cellular functions of MK2. *Mol Cell Biol*. 2002;22:4827-4835

984 78. Rousseau S, Dolado I, Beardmore V, Shpiro N, Marquez R, Nebreda AR, Arthur JS, Case
985 LM, Tessier-Lavigne M, Gaestel M*, et al.* CXCL12 and C5a trigger cell migration via a
986 PAK1/2-p38alpha MAPK-MAPKAP-K2-HSP27 pathway. *Cell Signal*. 2006;18:1897-1905

987 79. Jagielska J, Kapopara PR, Salguero G, Scherr M, Schutt H, Grote K, Schieffer B,
988 Bavendiek U. Interleukin-1 assembles a proangiogenic signaling module consisting of
989 caveolin-1, tumor necrosis factor receptor-associated factor 6, p38-mitogen-activated

protein kinase (MAPK), and MAPK-activated protein kinase 2 in endothelial cells. *Arterioscler Thromb Vasc Biol*. 2012;32:1280-1288

80. Ronkina N, Gaestel M. MAPK-Activated Protein Kinases: Servant or Partner? *Annu Rev Biochem*. 2022

81. Kapopara PR, von Felden J, Soehnlein O, Wang Y, Napp LC, Sonnenschein K, Wollert KC, Schieffer B, Gaestel M, Bauersachs J*, et al.* Deficiency of MAPK-activated protein kinase 2 (MK2) prevents adverse remodelling and promotes endothelial healing after arterial injury. *Thromb Haemost*. 2014;112:1264-1276

82. Limbourg A, von Felden J, Jagavelu K, Krishnasamy K, Napp LC, Kapopara PR, Gaestel M, Schieffer B, Bauersachs J, Limbourg FP*, et al.* MAP-kinase activated protein kinase 2 links endothelial activation and monocyte/macrophage recruitment in arteriogenesis. *PLoS One*. 2015;10:e0138542

83. Chen Y, Yang W, Zhang X, Yang S, Peng G, Wu T, Zhou Y, Huang C, Reinach PS, Li W*, et al.* MK2 inhibitor reduces alkali burn-induced inflammation in rat cornea. *Sci Rep*. 2016;6:28145

84. Neininger A, Kontoyiannis D, Kotlyarov A, Winzen R, Eckert R, Volk HD, Holtmann H, Kollias G, Gaestel M. MK2 targets AU-rich elements and regulates biosynthesis of tumor necrosis factor and interleukin-6 independently at different post-transcriptional levels. *J Biol Chem*. 2002;277:3065-3068

1009 85. Wu Y, He H, Ding Y, Liu S, Zhang D, Wang J, Jiang H, Zhang D, Sun L, Ye RD*, et al.*
1010 MK2 mediates macrophage activation and acute lung injury by regulating let-7e miRNA.
1011 *Am J Physiol Lung Cell Mol Physiol*. 2018;315:L371-L381

1012 86. Ba M, Rawat S, Lao R, Grous M, Salmon M, Halayko AJ, Gerthoffer WT, Singer CA.
1013 Differential regulation of cytokine and chemokine expression by MK2 and MK3 in airway
1014 smooth muscle cells. *Pulm Pharmacol Ther*. 2018;53:12-19

1015 87. Jaco I, Annibaldi A, Lalaoui N, Wilson R, Tenev T, Laurien L, Kim C, Jamal K, Wicky
1016 John S, Liccardi G*, et al.* MK2 Phosphorylates RIPK1 to Prevent TNF-Induced Cell Death.
1017 *Mol Cell*. 2017;66:698-710 e695

1018 88. Kulawik A, Engesser R, Ehlting C, Raue A, Albrecht U, Hahn B, Lehmann WD, Gaestel
1019 M, Klingmuller U, Haussinger D*, et al.* IL-1β-induced and p38(MAPK)-dependent
1020 activation of the mitogen-activated protein kinase-activated protein kinase 2 (MK2) in
1021 hepatocytes: Signal transduction with robust and concentration-independent signal
1022 amplification. *J Biol Chem*. 2017;292:6291-6302

1023 89. Shrestha A, Bruckmueller H, Kildalsen H, Kaur G, Gaestel M, Wetting HL, Mikkola I,
1024 Seternes OM. Phosphorylation of steroid receptor coactivator-3 (SRC-3) at serine 857 is
1025 regulated by the p38(MAPK)-MK2 axis and affects NF-kappaB-mediated transcription. *Sci*
1026 *Rep*. 2020;10:11388

1027 90. Ramachandran P, Pellicoro A, Vernon MA, Boulter L, Aucott RL, Ali A, Hartland SN,
1028 Snowdon VK, Cappon A, Gordon-Walker TT*, et al.* Differential Ly-6C expression

identifies the recruited macrophage phenotype, which orchestrates the regression of murine liver fibrosis. *Proc Natl Acad Sci U S A*. 2012;109:E3186-3195

91. Yu FF, Yang GH, Chen SB, Niu XL, Cai W, Tao YY, Wang XJ, Li M, Li YM, Zhao JH. Pseudolaric Acid B Attenuates High Salt Intake-Induced Hypertensive Left Ventricular Remodeling by Modulating Monocyte/Macrophage Phenotypes. *Med Sci Monit*. 2021;27:e932404

92. Hou X, Chen G, Bracamonte-Baran W, Choi HS, Diny NL, Sung J, Hughes D, Won T, Wood MK, Talor MV*, et al.* The Cardiac Microenvironment Instructs Divergent Monocyte Fates and Functions in Myocarditis. *Cell Rep*. 2019;28:172-189.e177

93. van Furth R, Diesselhoff-den Dulk MM. Dual origin of mouse spleen macrophages. *J Exp Med*. 1984;160:1273-1283

94. Mylonas KJ, Jenkins SJ, Castellan RF, Ruckerl D, McGregor K, Phythian-Adams AT, Hewitson JP, Campbell SM, MacDonald AS, Allen JE*, et al.* The adult murine heart has a sparse, phagocytically active macrophage population that expands through monocyte recruitment and adopts an 'M2' phenotype in response to Th2 immunologic challenge. *Immunobiology*. 2015;220:924-933

95. Horckmans M, Ring L, Duchene J, Santovito D, Schloss MJ, Drechsler M, Weber C, Soehnlein O, Steffens S. Neutrophils orchestrate post-myocardial infarction healing by polarizing macrophages towards a reparative phenotype. *Eur Heart J*. 2017;38:187-197

1048 96. Ray AL, Castillo EF, Morris KT, Nofchissey RA, Weston LL, Samedi VG, Hanson JA,
1049 Gaestel M, Pinchuk IV, Beswick EJ. Blockade of MK2 is protective in inflammation-
1050 associated colorectal cancer development. *Int J Cancer*. 2016;138:770-775

1051 97. Yu L, Song H, Fang X, Hu Y. Role of MK2 signaling pathway mediating
1052 microglia/macrophages polarization in chronic compression injury of cervical spinal cord.
1053 *Ann Palliat Med*. 2021;10:1304-1312

1054 98. Brown DI, Cooley BC, Quintana MT, Lander C, Willis MS. Nebulized Delivery of the
1055 MAPKAP Kinase 2 Peptide Inhibitor MMI-0100 Protects Against Ischemia-Induced
1056 Systolic Dysfunction. *Int J Pept Res Ther*. 2016;22:317-324

1057 99. Xu L, Yates CC, Lockyer P, Xie L, Bevilacqua A, He J, Lander C, Patterson C, Willis M.
1058 MMI-0100 inhibits cardiac fibrosis in myocardial infarction by direct actions on
1059 cardiomyocytes and fibroblasts via MK2 inhibition. *J Mol Cell Cardiol*. 2014;77:86-101

1060 100. Venugopal H, Hanna A, Humeres C, Frangogiannis NG. Properties and Functions of
1061 Fibroblasts and Myofibroblasts in Myocardial Infarction. *Cells*. 2022;11

1062 101. Tate M, Oseghale O, De Blasio MJ, Prakoso D, Qian H, Kiriazis H, Du XJ, Gregorevic P,
1063 Ritchie RH. Cardiac-selective bone morphogenetic protein 7 (BMP7) gene therapy to
1064 target cardiac fibrosis in a mouse model of diabetic cardiomyopathy. *Eur Heart J*. 2017;38

1065 102. Ong S, Rose NR, Cihakova D. Natural killer cells in inflammatory heart disease. *Clin*
1066 *Immunol*. 2017;175:26-33

1067 103. Upparahalli Venkateshaiah S, Niranjan R, Manohar M, Verma AK, Kandikattu HK, Lasky
1068 JA, Mishra A. Attenuation of Allergen-, IL-13-, and TGF-α-induced Lung Fibrosis after
1069 the Treatment of rIL-15 in Mice. *Am J Respir Cell Mol Biol*. 2019;61:97-109

1070 104. Manohar M, Kandikattu HK, Verma AK, Mishra A. IL-15 regulates fibrosis and
1071 inflammation in a mouse model of chronic pancreatitis. *Am J Physiol Gastrointest Liver*
1072 *Physiol*. 2018;315:G954-G965

1073 105. Fuchshofer R, Yu AH, Welge-Lussen U, Tamm ER. Bone morphogenetic protein-7 is an
1074 antagonist of transforming growth factor-beta2 in human trabecular meshwork cells. *Invest*
1075 *Ophthalmol Vis Sci*. 2007;48:715-726

1076 106. Biernacka A, Dobaczewski M, Frangogiannis NG. TGF-β signaling in fibrosis. *Growth*
1077 *Factors*. 2011;29:196-202

1078 107. Liu G, Ma C, Yang H, Zhang PY. Transforming growth factor beta and its role in heart
1079 disease. *Exp Ther Med*. 2017;13:2123-2128

1080 108. Schafer S, Viswanathan S, Widjaja AA, Lim WW, Moreno-Moral A, DeLaughter DM, Ng
1081 B, Patone G, Chow K, Khin E*, et al.* IL-11 is a crucial determinant of cardiovascular
1082 fibrosis. *Nature*. 2017;552:110-115

1083 109. Fernandez-Ruiz I. Cardioprotection: IL-11 is a potential therapeutic target in
1084 cardiovascular fibrosis. *Nat Rev Cardiol*. 2018;15:1

1085

Table 1. Echocardiography parameters of LV structure and function in 12-week-old MK2$^{+/+}$ and MK2$^{-/-}$ mice at 3 or 5 days post-MI.

	3 days post-MI				5 days post-MI			
	Sham		MI		Sham		MI	
	MK2$^{+/+}$	MK2$^{-/-}$	MK2$^{+/+}$	MK2$^{-/-}$	MK2$^{+/+}$	MK2$^{-/-}$	MK2$^{+/+}$	MK2$^{-/-}$
n	17	19	16	20	20	17	23	19
R-R interval, ms	181 [173, 217]	216 [186, 244]$	160 [149, 192] (15)	193 [178, 208]*	183 [166, 208]	204 [173, 247]	164 [150, 174]*	192 [167, 230]$
LV structure								
$LVAW_d$, mm	0.779 [0.743, 0.838]	0.784 [0.716, 0.846]	0.851 [0.656, 0.943]	0.790 [0.677, 0.906]	0.807 [0.760, 0.857]	0.744 [0.725, 0.788]	0.758 [0.627, 0.835]	0.746 [0.659, 0.890]
$LVPW_d$, mm [b]	0.737 [0.670, 0.779]	0.731 [0.621, 0.747]	0.804 [0.676, 0.973]	0.734 [0.619, 0.897]	0.730 [0.670, 0.808]	0.680 [0.643, 0.746]	0.734 [0.671, 0.818]	0.763 [0.726, 0.891]†
LVD_d, mm [b]	4.11 [3.78, 4.21]	3.89 [3.52, 4.07]	4.45 [3.96, 5.05]	4.18 [3.82, 4.52]*	4.05 [3.87, 4.24]	3.90 [3.83, 4.09]	4.94 [4.61, 5.29]¥	4.49 [4.26, 4.73]‡§
LVD_s, mm [b]	2.74 [2.37, 2.93]	2.38 [2.15, 2.76]	3.46 [3.12, 4.13]‡	3.35 [2.91, 3.64]¥	2.71 [2.58, 2.88]	2.47 [2.32, 2.84]	4.00 [3.54, 4.53]¥	3.56 [3.33, 3.94]¥ξ
LV mass, mg	110 [103, 118]	94.8 [90.0, 108]	141 [106, 192]*	117 [101, 135]*	114 [105, 127]	96.1 [93.7, 107]	149 [134, 167]¥	143 [114, 152]¥
LV mass/LVD_d, mg/mm	27.3 [25.4, 30.2]	26.4 [23.3, 27.8]	30.5 [27.2, 40.9]*	28.2 [25.0, 32.5]	28.2 [25.9, 30.0]	25.3 [24.1, 26.6]	31.1 [28.9, 33.8]	30.5 [27.0, 33.4]¥
BW, g	28.1 [26.1, 30.2]	24.5 [22.3, 26.0]$	27.3 [24.2, 31.0]	26.3 [23.9, 29.0]	29.9 [26.7, 33.7]	27.2 [25.3, 31.3]	28.0 [25.4, 31.3]	27.4 [25.8, 28.5]
LV mass/BW, mg/g	3.96 [3.81, 4.15]	4.11 [3.49, 4.29]	4.83 [4.13, 6.56]†	4.48 [3.79, 5.15]	3.79 [3.57, 4.04]	3.53 [3.17, 3.86]	5.34 [4.71, 5.90]¥	5.05 [4.27, 6.04]¥
LV systolic function								
LVFS, %	32.5 [30.1, 36.4]	37.7 [29.4, 39.9]	19.8 [13.7, 25.7]¥	20.0 [16.3, 24.6]¥	33.0 [29.5, 39.4]	38.5 [26.8, 40.5]	18.8 [11.4, 24.0]¥	18.9 [16.6, 24.7]¥
LVEF, %	67.7 [64.2, 73.0]	74.7 [63.5, 77.1]	46.7 [34.3, 57.3]¥	47.4 [39.9, 55.5]¥	68.5 [63.3, 76.5]	75.4 [59.2, 77.7]	44.6 [29.0, 54.2]¥	45.1 [40.5, 55.6]‡
LVV_d, μl [b]	173 [136, 186]	147 [111, 169]	218 [156, 310]*	182 [141, 257]*	166 [145, 188]	149 [141, 170]	291 [240, 353]¥	223 [191, 257]†§
LVV_s, μl	54.0 [35.5, 65.5]	36.0 [27.0, 55.0]	106 [78.3, 176]‡	96.5 [64.3, 123]¥	52.5 [45.0, 62.3]	40.0 [33.0, 59.5]	160 [113, 227]¥	115 [95.0, 154]*ξ
SV, μl	32.0 [29.3, 35.0](16)	28.0 [25.0, 33.0]	25.0 [22.0, 28.0](15)*	25.5 [18.0, 31.3]	34.0 [29.0, 40.0](19)	36.0 [28.5, 39.5]	25.0 [21.0, 32.0]‡	21.5 [18.0, 31.3]†
CO, ml/min	10.4 [8.83, 11.9](16)	7.82 [6.54, 10.5]$	9.73 [6.93, 11.8](15)	8.31 [6.04, 9.25]	11.9 [9.85, 13.9](19)	8.76 [8.15, 12.3]	9.42 [7.25, 11.15]*	6.88 [5.78, 9.20]*
S_L, cm/s	2.17 [1.86, 2.62]	2.17 [1.74, 2.30](18)	1.79 [1.49, 2.13](15)	1.73 [1.51, 1.98]	2.06 [1.68, 2.72]	2.21 [1.86, 2.36]	1.69 [1.43, 1.95]†	1.56 [1.35, 1.95]†
S_S, cm/s	2.38 [2.08, 2.51]	2.22 [2.06, 2.53](18)	2.08 [1.82, 2.23](15)	1.97 [1.68, 2.26]	2.61 [2.46. 3.10]	2.38 [2.08, 2.64]	2.20 [2.00, 2.58]*	1.89 [1.69, 2.20]*$
WMSI	1.00 [1.00, 1.00]	1.00 [1.00, 1.00]	1.67 [1.50, 1.95]¥	1.67 [1.50, 1.96]¥	1.00 [1.00, 1.00]	1.00 [1.00, 1.00]	1.67 [1.67, 2.33]¥	1.80 [1.67, 2.00]¥

LV diastolic function

Transmitral flow

E, cm/s [a]	71.8 [64.0, 78.1]	68.4 [63.6, 77.4]	66.8 [56.6, 79.6](15)	79.5 [70.4, 83.8]$	82.5 [71.1, 88.5]	80.7 [74.2, 88.7]	72.7 [64.9, 81.3]	67.4 [63.2, 79.2]
EDT, ms	37.0 [30.9, 39.9]	41.8 [34.2, 47.8]	32.6 [28.4, 36.7](15)	36.2 [29.0, 38.3]*	34.3 [28.1, 39.4]	39.6 [34.2, 45.3]	32.3 [26.8, 40.6]	34.2 [30.1, 43.6]
ED rate, m/s^2	20.0 [16.5, 22.7]	17.9 [14.6, 19.6]	24.1 [15.6, 27.8](15)	22.2 [18.6, 26.4]†	23.8 [20.5, 29.3]	19.1 [16.7, 25.4]	22.5 [15.9, 28.2]	19.3 [16.0, 26.1]
A, cm/s	47.2 [42.5, 50.7](16)	41.2 [34.1, 48.7](18)	30.8 [27.3, 40.1](10)	21.6 [12.2, 34.2](19)¥	47.2 [43.4, 54.1](19)	48.0 [43.1, 53.3]	35.1 [18.1, 47.7](16)†	25.3 [18.8, 49.0](16)†
E/A [a]	1.54 [1.31, 1.70](16)	1.63 [1.46, 1.80](18)	1.78 [1.51, 2.62](9)	3.90 [2.04, 5.96](19)¥$	1.60 [1.49, 1.80](19)	1.60 [1.49, 1.93]	1.85 [1.56, 4.15](16)*	2.28 [1.51, 4.06](16)*
Lateral Em, cm/s	1.61 [1.31, 2.03]	1.65 [1.34, 2.23](18)	1.33 [1.17, 1.66](10)	1.53 [1.43, 1.76](19)	0.90 [0.79, 1.02]	1.00 [0.92, 1.06]	0.97 [0.84, 1.09]	1.00 [0.71, 1.16]
Lateral Am, cm/s	1.93 [1.52, 2.31]	1.52 [1.43, 1.76](18)	1.08 [0.99, 1.40](10)‡	1.19 [1.09, 1.46](19)†	1.73 [1.24, 2.10](19)	1.80 [1.56, 2.11]	1.14 [0.94, 1.52](18)†	1.04 [0.80, 1.41](17)¥
Lateral Em/Am	0.85 [0.68, 1.05]	1.02 [0.85, 1.42](18)	1.05 [0.88, 1.73](10)	1.32 [0.97, 1.50](19)	0.99 [0.73, 1.51](19)	1.10 [0.87, 1.31]	1.30 [1.06, 1.55](18)	1.44 [1.04, 1.85](17)
Lateral E/Em	46.0 [35.2, 51.0]	38.3 [29.6, 51.7](18)	48.5 [44.5, 61.2](10)	51.5 [44.3, 56.1](19)*	44.1 [36.7, 60.2](19)	39.5 [35.0, 44.4]	44.9 [39.3, 56.2](18)	45.8 [40.2, 60.4](17)
Septal Em, cm/s	2.33 [1.89, 2.70]	2.18 [1.84, 2.74](18)	1.86 [1.53, 2.05](10)	1.92 [1.64, 2.22](19)	2.66 [2.18, 3.18](19)	2.34 [2.09, 2.65]	1.91 [1.77, 2.16](17)¥	1.69 [1.55, 1.83](17)†
Septal Am, cm/s	2.19 [1.89, 2.57]	2.02 [1.53, 2.20](18)	1.44 [1.06, 1.77](10)*	1.40 [1.22, 1.92](19)	2.40 [2.04, 2.55](19)	2.44 [1.85, 2.89]	1.62 [1.11, 2.23](17)*	1.41 [1.01, 1.84](17)¥
Septal Em/Am	1.01 [0.83, 1.23]	1.19 [0.89, 1.49](18)	1.18 [1.03, 1.69](10)	1.23 [0.94, 1.39]	1.23 [0.97, 1.51](19)	0.99 [0.87, 1.14]	1.06 [0.89, 1.78](17)	1.13 [1.06, 1.27]
Septal E/Em	30.4 [26.6, 39.1]	30.8 [23.5, 39.7](18)	38.6 [30.9, 42.9](10)	39.6 [34.2, 47.5](19)†	31.3 [25.7, 35.2](19)	34.9 [30.4, 39.0]	37.4 [30.2, 48.7](17)*	40.7 [34.0, 47.8](17)

Pulmonary venous flow

Upper S, cm/s	17.1 [15.1, 20.4](16)	14.5 [11.0, 18.7]	13.3 [5.76, 14.1](14)	9.72 [0.00.15.6]*	17.7 [15.0, 22.6]	17.9 [14.0, 22.9]	13.3 [8.56, 22.1]	9.00 [0.00, 17.4]‡
Upper D, cm/s [a]	44.5 [40.2, 48.3](16)	35.3 [30.9, 37.9](18)§	28.8 [25.0, 31.6](16)¥	30.9 [26.2, 35.0]	46.7 [38.2, 49.3]	33.5 [32.7, 37.9]§	32.3 [30.3, 40.00]¥	26.7 [24.5, 31.3]*$
Upper S/D	0.39 [0.34, 0.42](16)	0.45 [0.36, 0.55](18)	0.36 [0.21, 0.49](16)	0.33 [0.00, 0.56]	0.41 [0.32, 0.51]	0.56 [0.40, 0.63]$	0.43 [0.28, 0.56]	0.34 [0.00, 0.64]
Lower S, cm/s	46.9 [39.4, 53.0](16)	41.8 [31.2, 47.3](17)	37.3 [30.4, 41.6](15)*	36.0 [30.8, 45.5]	49.1 [45.0, 59.2]	44.5 41.3, 53.2	45.6 [34.5, 54.7]	36.7 [23.0, 43.3]*$
Lower D, cm/s	30.9 [27.0, 37.3](16)	28.3 [25.4, 36.6](17)	21.4 [15.6, 22.5](15)‡	25.7 [18.4, 28.7]*	37.6 [27.0, 44.6]	31.5 [24.9, 36.3]	31.1 [23.6, 34.1]*	23.4 [18.7, 30.7]
Lower S/D	1.49 [1.30, 1.70](16)	1.44 [1.18, 1.56](17)	1.77 [1.44, 1.93](15)‡	1.54 [1.26, 1.85]	1.32 [1.17, 1.68]	1.45 [1.36, 1.65]	1.42 [1.25, 1.69]*	1.39 [1.12, 2.02]
Mean S/D	0.93 [0.87, 1.05](16)	0.94 [0.81, 1.00](18)	1.06 [0.89, 1.13](16)	0.93 [0.73, 1.09]	0.90 [0.79, 1.02]	1.00 [0.92, 1.06]	0.97 [0.84, 1.09]	1.00 [0.71. 1.16]
S slope m/s^2	4.04 [3.17, 4.87](16)	3.14 [2.61, 3.59](17)	3.53 [3.17, 4.65](15)	3.56 [2.71, 4.31]	4.32 [3.02, 5.20]	3.33 [2.80, 4.03]	4.63 [3.61, 5.38]	3.05 [2.73, 4.69]

LV isovolumetric relaxation time								
IVRTc	0.87 [0.77, 1.00]	0.84 [0.75, 1.11]	1.23 [0.90, 1.34](15)	1.00 [0.77, 1.10]	0.86 [0.74, 1.13](19)	0.99 [0.70, 1.16]	1.05 [0.78, 1.42]	1.21 [0.86, 1.39](18)
LA dimensions								
LAD_s, mm	2.02 [1.92, 2.34]	2.13 [1.81, 2.24]	2.51 [2.18, 2.68](15)*	2.26 [2.01, 2.37]‡	2.15 [1.99, 2.32]	2.01 [1.84, 2.26]	2.60 [2.27, 2.93]‡	2.18 [2.02, 2.38]¥
LAD_d, mm	1.68 [1.49, 1.90]	1.64 [1.51, 1.75]	2.01 [1.78, 2.47](15)†	2.25 [1.85, 2.50]¥	1.74 [1.55, 1.97]	1.58 [1.50, 1.90]	2.26 [1.95, 2.63]¥	2.41 [2.08, 2.64]¥
LAFS, %	20.3 [14.5, 21.8]	19.7 [15.2, 25.4]	14.9 [8.87, 19.8](15)	11.0 [7.73, 14.4]¥	19.1 [16.2, 24.7]	17.0 [14.6, 21.7]	11.5 [8.87, 15.6]¥	12.3 [9.99, 15.0]*
MPI								
Septal MPI, %	52.6 [44.0, 57.4]	52.6 [44.5, 59.7](18)	80.3 [54.9, 106](15)‡	69.4 [52.6, 85.7]*	54.0 [44.4, 63.3]	49.6 [42.7, 60.0]	75.4 [63.0, 95.6]¥	71.3 [59.4, 85.5]¥
Lateral MPI, %	53.1 [45.8, 56.6]	52.7 [43.3, 60.6](18)	90.4 [66.2, 106](15)¥	75.7 [52.2, 91.7]†	51.4 [46.4, 58.6]	50.2 [45.4, 59.5]	73.0 [61.5, 94.0]‡	75.0 [53.4, 90.5]‡
Global MPI, %	45.0 [35.1, 53.3]	42.7 [38.5, 52.6]	66.3 [48.4, 98.0](15)‡	66.2 [46.9, 78.9]†	39.2 [33.6, 48.9](19)	44.4 [36.2, 51.6]	62.1 [50.9, 92.1]¥	74.4 [60.9, 89.6](18)¥

Data are reported as median [1st quartile, 3rd quartile]. The *n* numbers are as shown in the first row of the table unless otherwise indicated in parentheses. A indicates trans mitral flow late (atrial) filling velocity; A_m, mitral annulus peak velocity during atrial diastolic filing; BW, body weight; CO, cardiac output; D, peak velocity during pulmonary venous diastolic flow; E, transmitral flow early filling velocity; ED, E wave deceleration; EDT, E wave deceleration time; E_m, mitral annulus peak velocity during early diastolic filling; IVRT, isovolumic relaxation time; IVRTc: heart rate-corrected IVRT; LAD_d, left atrium dimension at end cardiac diastole; LAD_s, left atrium dimension at end cardiac systole; LAFS, left atrium fractional shortening; LV, left ventricular; $LVAW_d$, left ventricular anterior wall thickness at end cardiac diastole; LVD_d, left ventricular dimension at end cardiac diastole; LVD_s, left ventricular dimension at end cardiac systole; LVEF, left ventricular ejection fraction; LVFS, left ventricular fractional shortening; $LVPW_d$, left ventricular posterior wall thickness at end cardiac diastole; LVV_d, left ventricular volume at end cardiac diastole; LVV_s, left ventricular volume at end cardiac systole; MK2, mitogen-activated protein kinase–activated protein kinase-2; MPI, myocardial performance index; S, peak velocity during pulmonary venous systolic flow; SD, slope: pulmonary venous systolic flow decelerating slope; S_L, basal lateral systolic velocity; S_S, basal septal systolic velocity; SV, stroke volume; and WMSI, wall motion score index. Shapiro-Wilk tests for normality were performed for all data: if a lognormal distribution was indicated, data was log-transformed prior to statistical comparison by two-way ANOVA, including a factor for surgery (sham, MI), a factor for genotype ($MK2^{+/+}$, $MK2^{-/-}$), and a surgery x genotype interaction term. The ANOVA was followed by Tukey's post hoc tests for multiple comparisons to compare means. *: $P < 0.05$ vs sham. †: $P < 0.01$ vs sham. ‡: $P < 0.001$ vs sham. ¥: $P < 0.0001$ vs sham. $: $P < 0.05$ vs $MK2^{+/+}$. ξ: $P < 0.01$ vs $MK2^{+/+}$. §: $P < 0.001$ vs $MK2^{+/+}$. [a]: $P < 0.05$ for surgery x genotype interaction 3-days post-MI. [b]: $P < 0.05$ for surgery x genotype interaction 5-days post-MI.

Table 2. Echocardiographic parameters of RV structure and function in 12-week-old $MK2^{+/+}$ and $MK2^{-/-}$ mice at 3 or 5 days post-MI.

	3 days post-MI				5 days post-MI			
	Sham		MI		Sham		MI	
	$MK2^{+/+}$	$MK2^{-/-}$	$MK2^{+/+}$	$MK2^{-/-}$	$MK2^{+/+}$	$MK2^{-/-}$	$MK2^{+/+}$	$MK2^{-/-}$
n	17	19	16	20	20	17	23	19
RV structure								
$RVAW_d$, mm	0.311 [0.239, 0.334]	0.297 [0.261, 0.322]	0.334 [0.264, 0.373]	0.30 [0.26, 0.32](19)	0.329 [0.297, 0.357]	0.319 [0.297, 0.351]	0.359 [0.275, 0.396]	0.359 [0.276, 0.392]
RVD_d, mm [a]	1.61 [1.57, 1.79]	1.73 [1.54, 1.84]	1.82 [1.69, 1.94]	1.67 [1.60, 1.79]	1.87 [1.70, 2.01]	1.81 [1.58.1.95]	1.70 [1.55, 1.92]	1.77 [1.57, 1.91]
$RVAW_d/RVD_d$	0.18 [0.15, 0.19]	0.17 [0.16, 0.19]	0.17 [0.16, 0.20]	0.18 [0.16, 0.21](19)	0.17 [0.15, 0.18]	0.18 [0.16, 0.20]	0.19 [0.17, 0.21]	0.20 [0.16, 0.23]
RV Systolic Function								
TAPSE, mm	1.21 [1.10, 1.26]	1.22 [1.13, 1.39]	1.04 [0.93, 1.12](15)*	1.04 [0.97, 1.18]†	1.34 [1.17, 1.45](19)	1.24 [1.13, 1.31]	1.03 [0.88, 1.13]¥	1.02 [0.95, 1.08]†
S_R, cm/s	2.97 [2.60, 3.72]	2.77 [2.36, 3.32]	2.64 [2.01, 3.29](15)	2.11 [1.68,2.54]†	3.58 [2.77, 4.26]	3.10 [2.73, 3.58]	2.45 [2.25, 2.87]¥	2.31 [2.01, 2.49]†
RV Diastolic function								
Transtricuspid flow								
E_t, cm/s [a]	24.4 [21.2, 28.1]	28.6 [25.3, 33.1]	37.6 [23.7, 43.2](15)†	25.9 [21.3, 29.0]ξ	28.6 [24.3, 34.2]	25.0 [21.8, 27.9]	32.2 [28.6, 41.4]	30.2 [23.8, 36.3]
E_tDT, ms	29.0 [24.8, 38.6]	38.7 [36.5, 46.7]	31.9 [21.5, 34.9](15)	30.3 [22.4, 38.6]†	29.8 [25.8, 36.3]	35.4 [27.3. 40.5]	28.3 [24.4, 39.7]	29.2 [24.5, 35.3]
E_tD rate, m/s^2	8.76 [6.32, 9.66]	7.34 [6.26, 8.85]	11.8 [9.90, 14.0](15)‡	7.76 [6.48, 11.6]ξ	9.89 [7.55, 14.0]	7.31 [6.52, 9.07]	13.5 [9.78, 16.1]	9.38 [7.24, 14.0]
A_t, cm/s	39.6 [34.9, 45.1](16)	42.6 [38.5, 46.6](16)	40.1 [36.0, 47.1](6)	39.1 [35.4, 46.1](19)	42.0 [36.7, 45.6](16)	41.3 [38.1, 43.1](16)	41.6 [36.1, 45.2](11)	34.1 [27.6, 41.9](14)
E_t/A_t	0.57 [0.48, 0.76](16)	0.62 [0.59, 0.72](16)	0.56 [0.53, 0.66](6)	0.64 [0.57, 0.71](19)	0.68 [0.58, 0.75](16)	0.59 [0.50, 0.70](16)	0.75 [0.62, 0.82](11)	0.74 [0.56, 0.96](14)*
Lateral E_m, cm/s [b]	2.58 [2.11, 3.64](16)	2.30 [1.93, 2.58](17)	1.87 [1.42, 2.76](9)*	1.72 [1.50, 2.40]	3.27 [2.64, 3.66](18)	2.48 [1.94, 3.09](16)ξ	2.30 [1.79, 2.59](14)¥	2.18 [1.67, 2.38](18)
Lateral A_m, cm/s	3.02 [2.49, 3.61](16)	2.32 [1.75, 2.95](17)	2.79 [1.64, 3.45](9)	1.83 [1.17, 2.27]	2.86 [2.33, 3.55](18)	3.15 [2.75, 3.47](16)	1.50 [1.12, 2.65](14)†	2.10 [1.47, 2.81](18)†
Lateral E_m/A_m	0.94 [0.73, 1.30](16)	1.05 [0.81, 1.22] (17)	0.73 [0.59, 1.01](9)	1.27 [0.88, 1.38]	1.14 [0.93, 1.28](18)	0.90 [0.75, 1.01](16)	1.48 [0.93, 1.92](16)	1.01 [0.65, 1.43](18)
Lateral E_t/E_m [a]	8.99 [7.11, 11.7](16)	12.2 [10.4, 15.2](17)	17.5 [9.26, 22.7](9)‡	14.2 [10.7, 16.9]	9.13 [6.56, 10.6](18)	9.91 [7.89, 11.2](16)	12.9 [12.2, 17.2](14)¥	14.1 [11.4, 16.8](18)†

Pulmonary artery flow								
AT, ms	22.9 [18.9, 27.3]	24.6 [18.1, 29.1]	16.3 [14.6, 17.9]†	16.1 [13.8, 19.9](15)†	21.5 [18.4, 24.5](17)	24.6 [19.5, 29.8]	15.0 [13.3, 16.8](22)‡	16.1 [13.4, 19.5]‡
AT/RVET	30.3 [27.1, 35.4]	28.6 [23.9, 31.5]	22.5 [21.6, 26.7]†	21.6 [20.7, 26.4](15)	28.1 [25.0, 30.8](17)	29.2 [25.1, 31.6]	22.7 [16.8, 26.8](22)†	21.0 [18.9, 23.5]‡
RV MPI								
TV_{CO}, ms	96.3 [88.8, 106]	115 [104, 122]	98.8 [95.7, 116](15)	105 [88.0, 118](19)	97.9 [81.5, 109]	108 [88.2, 128]	96.9 [85.1, 106]	123 [104, 135]
RVET, ms	76.0 [67.4, 85.1]	85.9 [75.4, 98.0]	69.5 [64.9, 77.0]	74.3 [63.1, 81.6](16)†	72.6 [70.7, 82.1](17)	82.4 [72.6, 93.6]	66.2 [62.6, 76.7](22)	82.8 [67.8, 88.7]$
Lateral MPI, %	41.5 [35.6, 44.7]	42.3 [35.2, 49.8]	59.1 [43.3, 73.8](15)‡	51.0 [38.8, 56.4]	41.1 [35.3, 45.4]	38.7 [34.2, 46.6]	56.0 [48.6, 67.0]¥	56.6 [47.5, 69.3]¥
Global MPI, %	29.4 [22.0, 37.6]	31.5 [23.1, 37.6]	50.0 [30.9, 56.1](15)†	36.9 [31.1, 52.2](16)	27.4 [22.3, 39.2](17)	30.2 [18.7, 33.0]	39.7 [30.8, 55.1](22)*	48.4 [32.5, 56.0]‡

Data are reported as median [1st quartile, 3rd quartile]. The *n* numbers are as shown in the first row of the table unless otherwise indicated in parentheses. A_m, tricuspid annulus peak velocity during late (atrial) diastolic filing; AT, pulmonary arterial flow acceleration time; A_t, transtricuspid flow late (atrial) filling velocity; E_m, tricuspid annulus peak velocity during early diastolic filing; E_t, transtricuspid flow early filling velocity; E_tD rate, transtricuspid early filling deceleration rate; E_tDT, transtricuspid early filling deceleration time; MK2, mitogen-activated protein kinase–activated protein kinase-2; MPI, myocardial performance index; RV, right ventricular; $RVAW_d$, right ventricular anterior wall thickness at end cardiac diastole; RVD_d, right ventricular diameter at end cardiac diastole; RVET, right ventricular ejection time; S_R, right ventricular lateral wall systolic velocity; TAPSE, tricuspid annulus plane systolic excursion; and TV_{CO}; tricuspid valve closure to opening time. Shapiro-Wilk tests for normality were performed for all data: if a lognormal distribution was indicated, data was log-transformed prior to statistical comparison by two-way ANOVA, including a factor for surgery (sham, MI), a factor for genotype ($MK2^{+/+}$, $MK2^{-/-}$), and a surgery x genotype interaction term. The ANOVA was followed by Tukey's post hoc tests for multiple comparisons to compare means. *: $p < 0.05$ vs Sham. †: $p < 0.01$ vs Sham. ‡: $p < 0.001$ vs sham. ¥: $p < 0.0001$ vs Sham. $: $p < 0.05$ vs $MK2^{+/+}$. ξ: $p < 0.01$ vs $MK2^{+/+}$. §: $p < 0.001$ vs $MK2^{+/+}$. $^{+/+}$. [a]: $P < 0.05$ for surgery x genotype interaction 3-days post-MI. [b]: $P < 0.05$ for surgery x genotype interaction 5-days post-MI.

Table 3. Effect of MK2-deficiency on cytokine transcript abundance following MI.

gene		3 days post-MI				5 days post-MI			
		healthy tissue		infarct		healthy tissue		infarct	
		fold regulation	*P*	fold regulation	*P*	fold regulation	*P*	fold regulation	*P*
Adipoq		2.33	0.361	-2.10	0.077	-7.14	0.377	-1.88	0.255
Bmp2		-1.35	0.163	-1.64	0.272	1.28	0.197	-2.08	0.811
Bmp4		1.51	0.294	1.39	0.252	-1.68	0.226	-1.31	0.205
Bmp6		-1.14	0.526	1.54	0.455	1.1	0.466	-1.36	0.7478
Bmp7		-3.00	0.557	-1.01	0.161	1.51	0.520	1.25	0.460
Ccl1		**-1.03**	**0.045**	1.83	0.703	-1.68	0.803	-1.37	0.311
Ccl11		-1.08	0.245	-2.43	0.671	-5.08	0.947	-1.51	0.158
Ccl12		-1.25	0.503	-1.32	0.925	-1.88	0.727	-1.41	0.072
Ccl17		4.07	0.506	-1.91	0.557	1.12	0.145	2.55	0.703
Ccl19		1.10	0.453	1.69	0.599	1.3	0.374	2.18	0.628
Ccl2		-1.33	0.305	-2.81	0.465	1.29	0.310	1.87	0.947
Ccl20		**2.33**	**0.045**	1.83	0.077	-1.81	0.545	1.25	0.257
Ccl22		1.58	0.583	-1.05	0.557	-2.70	0.740	-1.42	0.411
Ccl24		-1.08	0.230	2.76	0.524	-1.70	0.458	1.48	0.413
Ccl3		**1.05**	**0.017**	-2.42	0.915	1.50	0.570	1.24	0.356
Ccl4		-1.58	0.185	-1.35	0.288	2.20	0.285	1.69	0.136
Ccl5		1.37	0.977	1.64	0.386	1.12	0.314	-1.27	0.574
Ccl7		1.06	0.426	-1.96	0.807	-1.25	0.309	2.37	0.575
Cd40lg		**2.48**	**0.045**	1.83	0.114	-2.07	0.430	1.57	0.300
Cd70		2.27	0.045	1.83	0.408	-2.31	0.545	1.25	0.361
Cntf		-1.67	0.122	1.76	0.076	-1.44	0.826	1.06	0.400
Csf1		-1.43	0.414	-1.26	0.171	1.18	0.469	-1.25	0.940
Csf2		5.03	0.574	-1.24	0.282	1.62	0.354	2.17	0.214
Csf3		-2.59	0.605	1.37	0.199	1.1	0.382	2.96	0.731
Ctf1		-3.16	0.754	-1.89	0.184	2.87	0.600	**1.19**	**0.028**
Cx3cl1		-1.25	0.990	1.31	0.436	2.09	0.588	1.09	0.091
Cxcl1		-4.11	0.394	-2.40	0.153	1.84	0.972	-1.39	0.244
Cxcl10		-1.1	0.082	-1.36	0.813	1.41	0.664	-1.09	0.601
Cxcl11		**2.48**	**0.025**	1.70	0.059	-1.20	0.895	-1.16	0.833
Cxcl12		-1.23	0.518	-1.12	0.297	-1.34	0.537	-1.17	0.360
Cxcl13		2.4	0.975	1.36	0.532	-2.71	0.366	-1.8	0.253
Cxcl16		1.08	0.471	1.52	0.854	-1.24	0.996	1.00	0.639
Cxcl3		-2.54	0.086	-4.82	0.341	-1.15	0.385	2.46	0.531
Cxcl5		-1.6	0.477	-1.68	0.412	-1.77	0.319	2.27	0.565
Cxcl9		4.69	0.503	2.29	0.191	**-1.21**	**0.0016**	3.93	0.943
Fasl		2.33	0.215	3.16	0.077	-2.72	0.545	1.25	0.070
Gpi1		-1.12	0.441	-13.42	0.657	-1.00	0.682	-1.05	0.976
Hc		1.05	0.096	1.59	0.598	2.76	0.509	-1.77	0.144
Ifna2		6.27	0.402	1.91	0.034	-1.53	0.618	-1.05	0.399
Ifng		**2.33**	**0.030**	1.82	0.077	-1.47	0.545	1.25	0.766
Il10		2.00	0.304	2.48	0.291	5.08	0.284	**2.57**	**0.039**
Il11		-2.42	0.516	-1.26	0.317	-4.45	0.445	-1.75	0.188
Il12a		2.95	0.650	1.46	0.274	-3.98	0.932	1.09	0.249
Il12b		4.22	0.689	1.05	0.237	-1.4	0.397	2.05	0.428
Il13		**1.79**	**0.045**	1.83	0.844	-1.71	0.446	1.49	0.089
Il15		-1.46	0.318	-2.09	0.289	**1.28**	**0.033**	-2.45	0.529
Il16		-2.51	0.174	**-2.29**	**0.0065**	1.96	0.281	-3.64	0.195

Il17a		4.18	0.848	1.27	0.131	-1.81	0.545	1.25	0.257
Il17f		2.88	0.242	2.05	0.105	-2.21	0.478	1.41	0.173
Il18		-1.37	0.225	-1.68	0.948	-1.61	0.559	-2.44	0.082
Il1a		1.84	0.443	1.44	0.200	-1.43	0.322	5.09	0.566
Il1b		-1.25	0.209	-1.57	0.536	1.04	0.274	6.34	0.953
Il1rn		**-1.35**	**0.020**	-2.68	0.439	1.85	0.779	-1.01	0.081
Il2		2.33	0.150	1.33	0.077	-1.81	0.545	1.25	0.257
Il21		**2.33**	**0.045**	1.83	0.077	-1.81	0.545	1.25	0.257
Il22		2.33	0.828	1.19	0.077	-1.81	0.545	1.25	0.257
Il23a		2.11	0.856	1.15	0.252	1.41	0.852	-1.27	0.619
Il24		**1.59**	**0.046**	1.76	0.983	-1.54	0.545	1.25	0.342
Il27		**1.88**	**7e-006**	10.26	0.8637	-1.29	0.203	-3.03	0.511
Il3		2.33	0.130	1.52	0.077	-1.81	0.545	1.25	0.257
Il4		4.73	0.121	1.53	0.335	1.54	0.545	1.25	0.485
Il5		2.15	0.420	2.10	0.121	-2.06	0.229	2.72	0.312
Il6		-2.28	0.139	-5.48	0.460	3.02	0.413	3.16	0.295
Il7		2.33	0.410	-1.48	0.281	1.1	0.230	2.44	0.818
Il9		**2.33**	**0.045**	1.83	0.077	-1.81	0.544	1.25	0.257
Lif		-1.28	0.272	-2.03	0.965	1.82	0.238	4.12	0.508
Lta		3.10	0.978	1.22	0.095	-1.66	0.261	1.74	0.607
Ltb		-2.24	0.709	1.22	0.288	1.16	0.457	-1.71	0.692
Mif		1.34	0.757	1.25	0.135	-1.56	0.829	1.08	0.071
Mstn		1.25	0.204	1.35	0.942	-1.35	0.492	1.35	0.566
Nodal		2.68	0.173	2.96	0.160	**-1.81**	**0.0090**	3.54	0.257
Osm		-1.16	0.101	-5.62	0.511	-1.41	0.417	-3.14	0.436
Pf4		-1.47	0.151	-15.28	0.459	-1.2	0.633	-1.21	0.646
Ppbp		-1.93	0.414	-1.28	0.369	-1.55	0.900	1.32	0.476
Spp1		-1.4	0.503	-1.48	0.228	-1.22	0.778	1.05	0.522
Tgfb2		1.5	0.096	-1.71	0.276	-1.24	0.385	-2.00	0.236
Thpo		1.65	0.255	2.45	0.916	1.55	0.817	-1.37	0.940
Tnf		-1.15	0.266	-2.06	0.854	-1.31	0.546	-2.93	0.491
Tnfrsf11b		1.18	0.585	-3.89	0.830	1.01	0.338	1.74	0.933
Tnfsf10		1.13	0.870	-1.40	0.648	1.23	0.244	1.37	0.224
Tnfsf11		**-2.79**	**0.012**	-6.71	0.363	-1.38	0.683	1.59	0.401
Tnfsf13b		-3.32	0.994	1.01	0.430	-1.13	0.394	-2.18	0.582
Vegfa		1.21	0.628	1.12	0.669	1.30	0.908	-1.02	0.614
Xcl1		3.06	0.616	1.33	0.406	**-1.95**	**0.010**	4.80	0.502

Data shown are expressed as the fold-regulation in transcript abundance relative to the respective values from $MK2^{+/+}$ hearts. Fold-regulation: Fold-change values greater than one indicate an increase in transcript abundance, relative to that of $MK2^{+/+}$ cardiac tissue, and the fold-regulation is equal to the fold-change. Where the transcript abundance is less than that of $MK2^{+/+}$ cardiac tissue, the fold-change is less than one and the fold-regulation is the negative inverse of the fold-change. Cells where $P < 0.05$ are indicated in bold. n = 3 - 4.

Figure 1

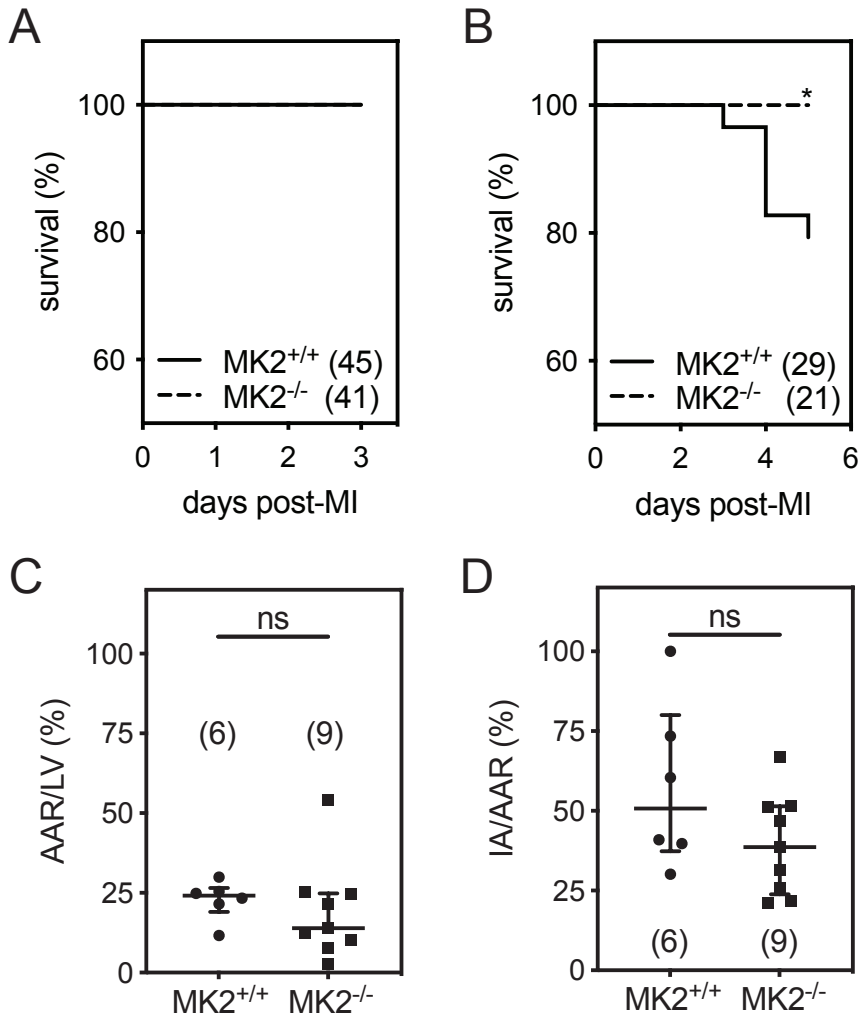

Figure 2

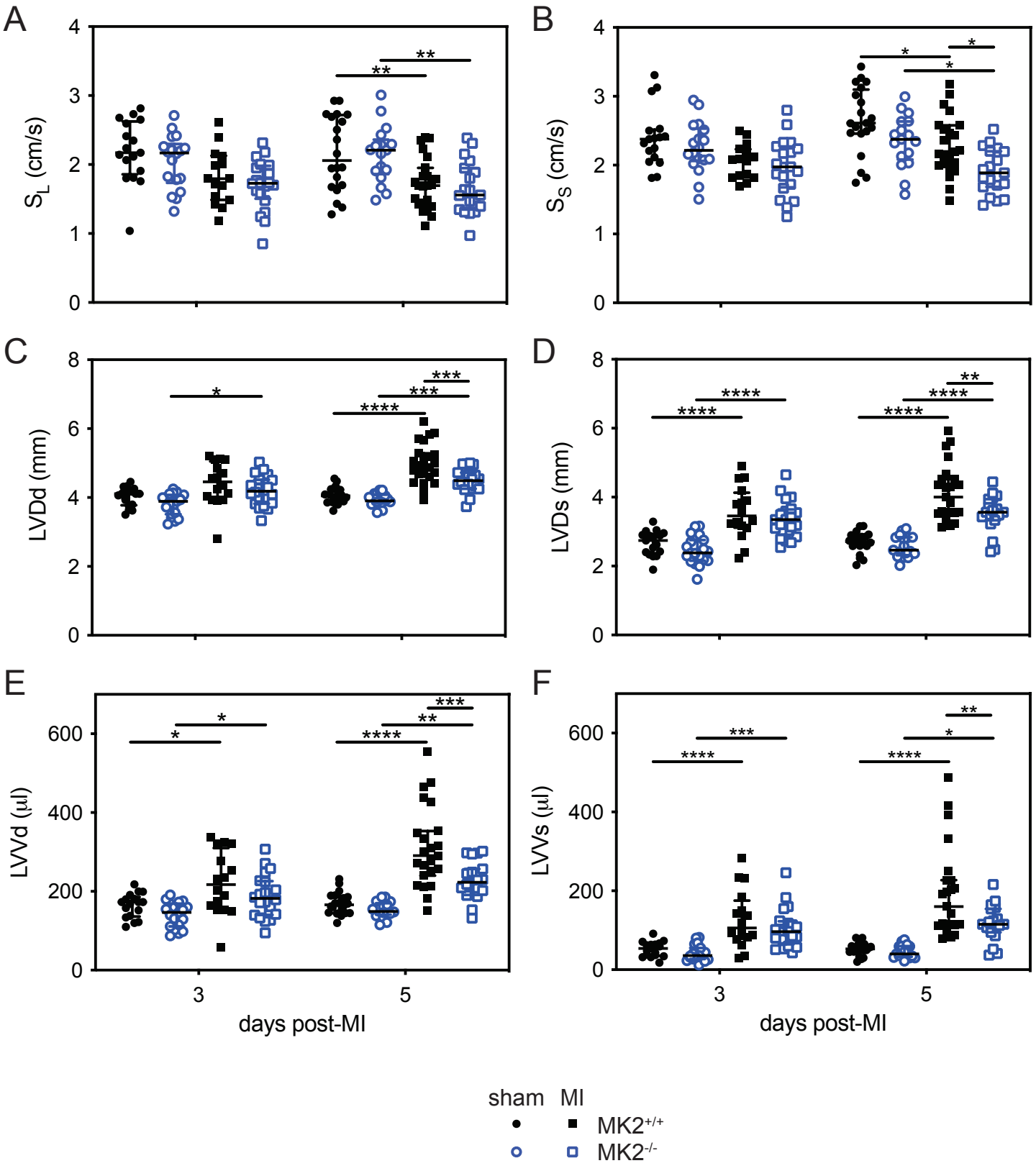

Figure 3

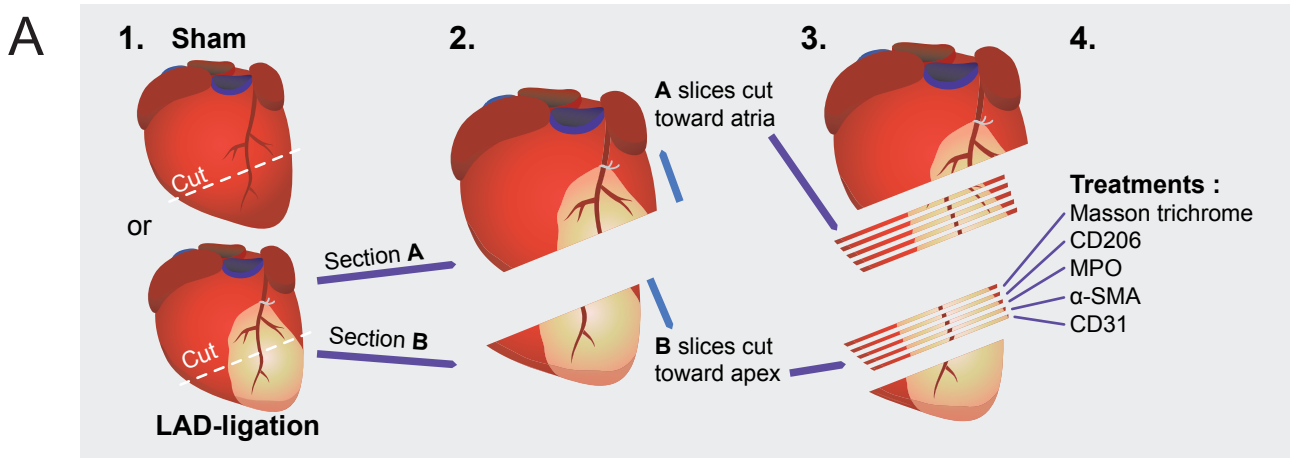

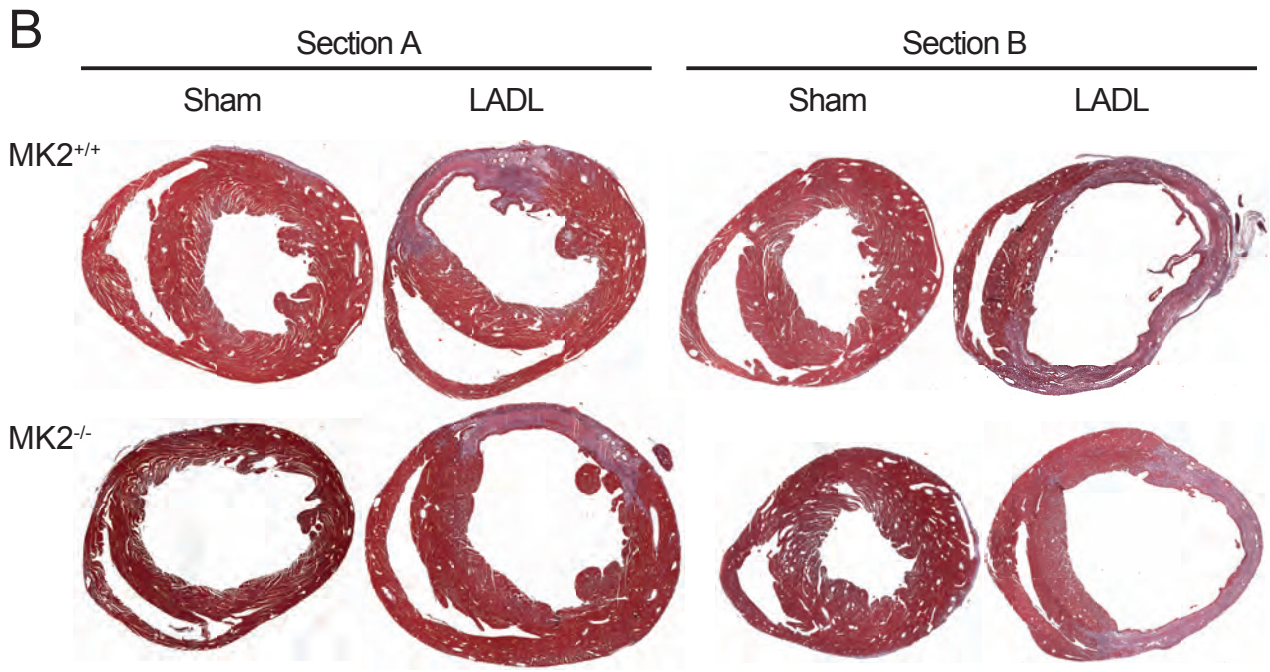

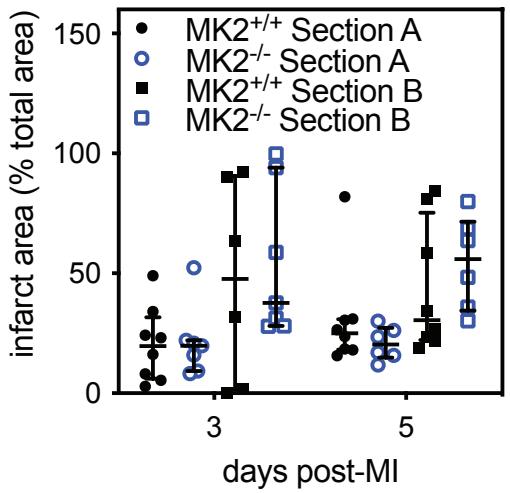

Figure 4

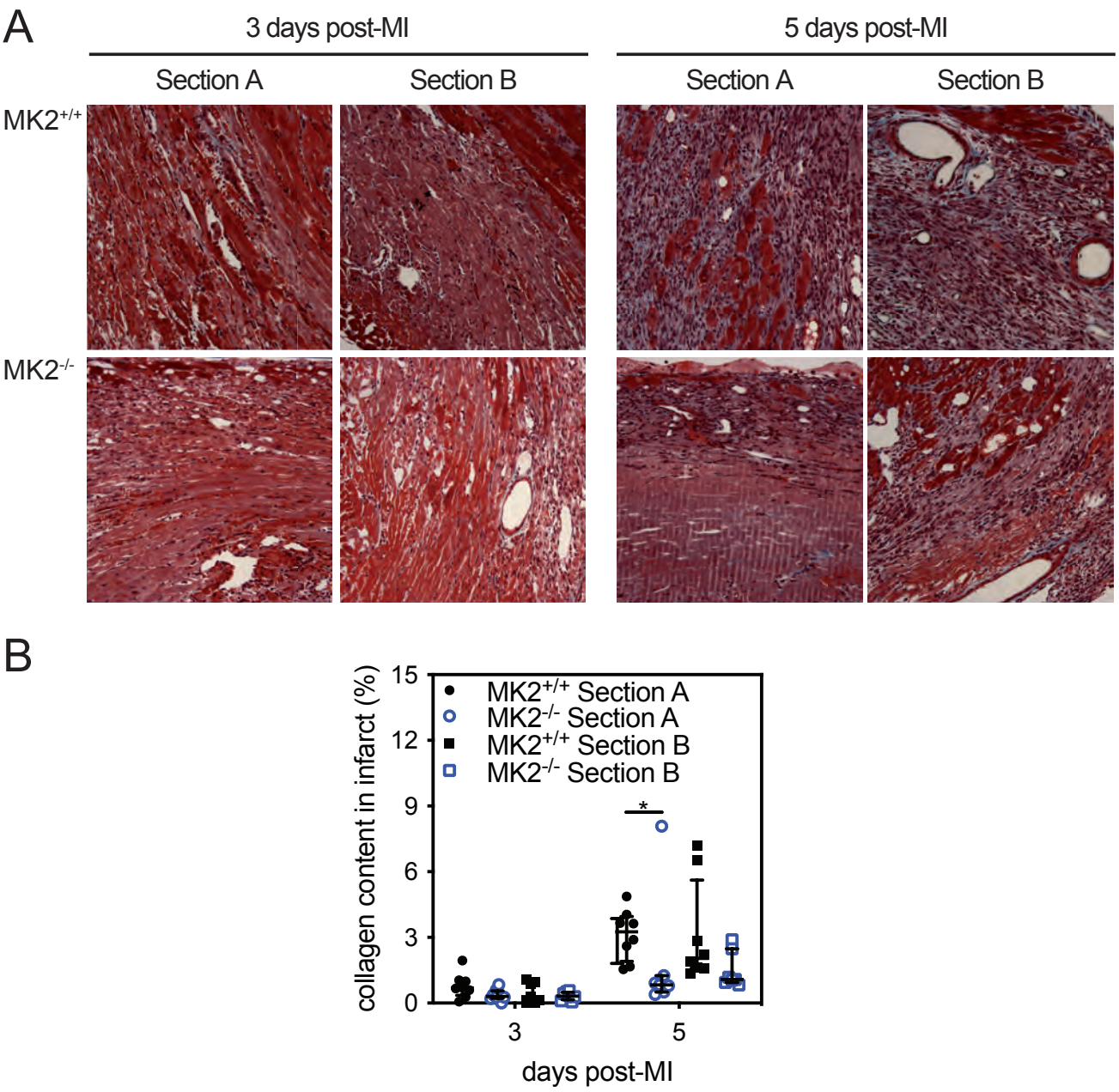

Figure 5

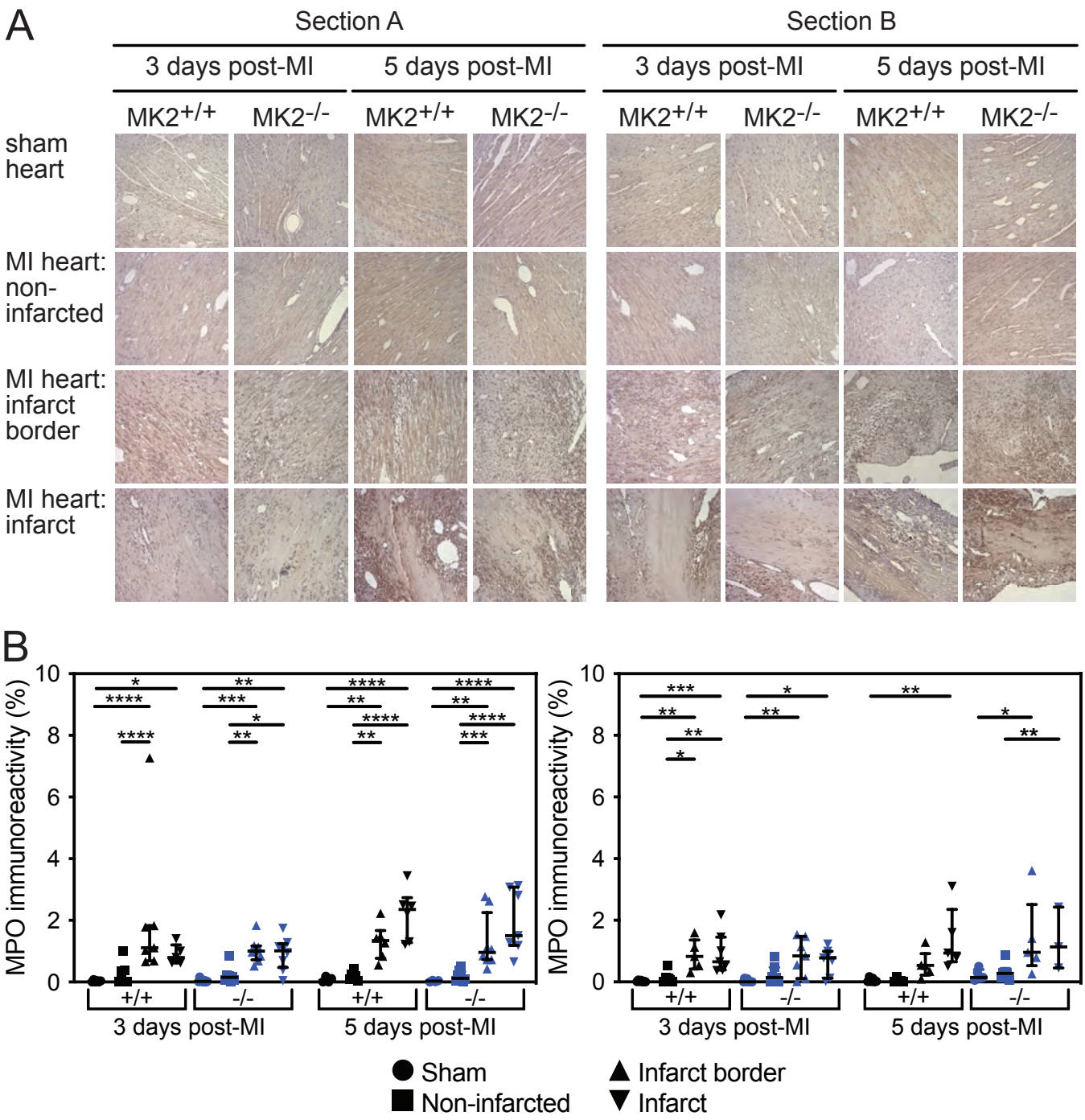

Figure 6

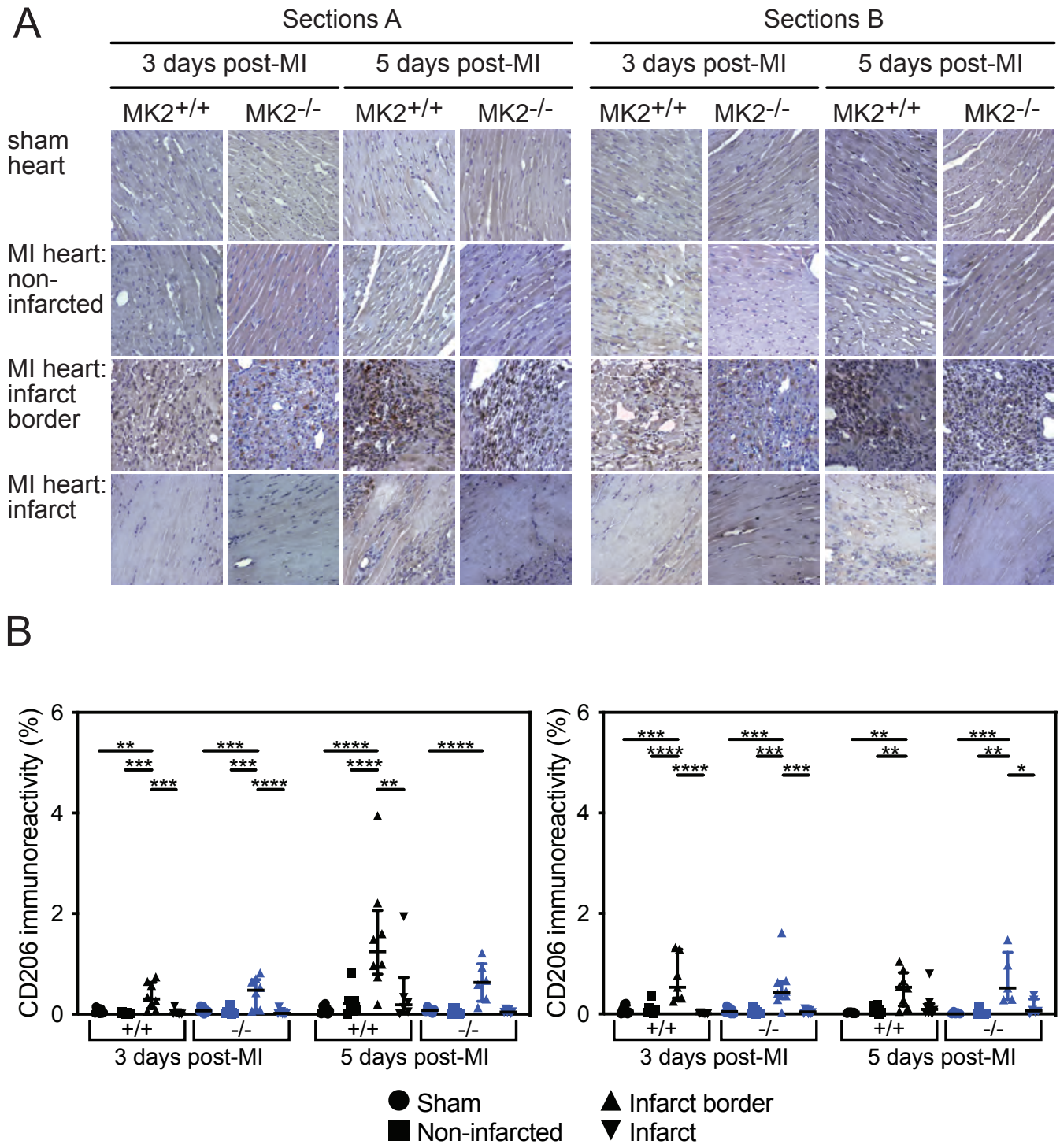

Figure 7

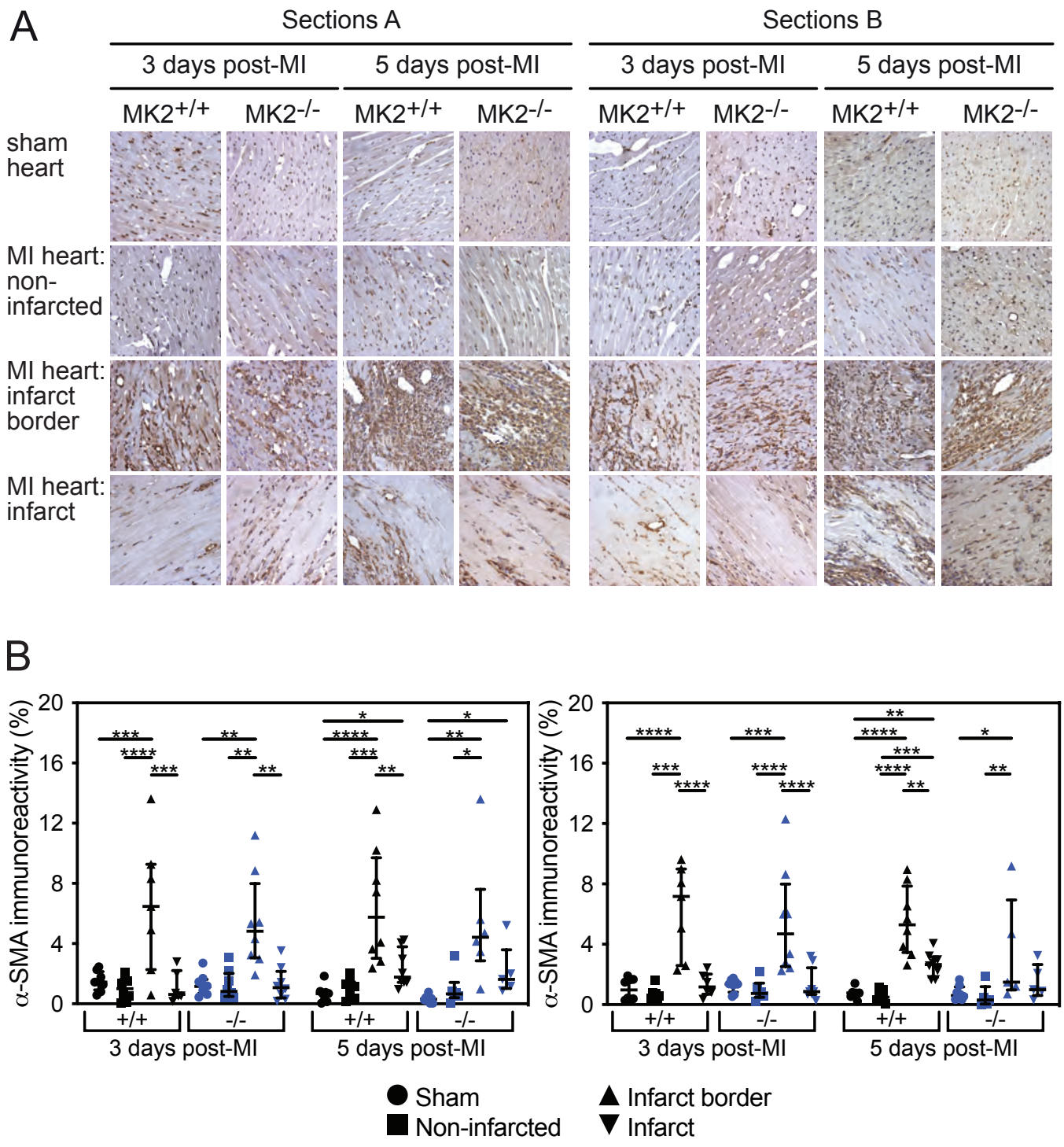

Figure 8

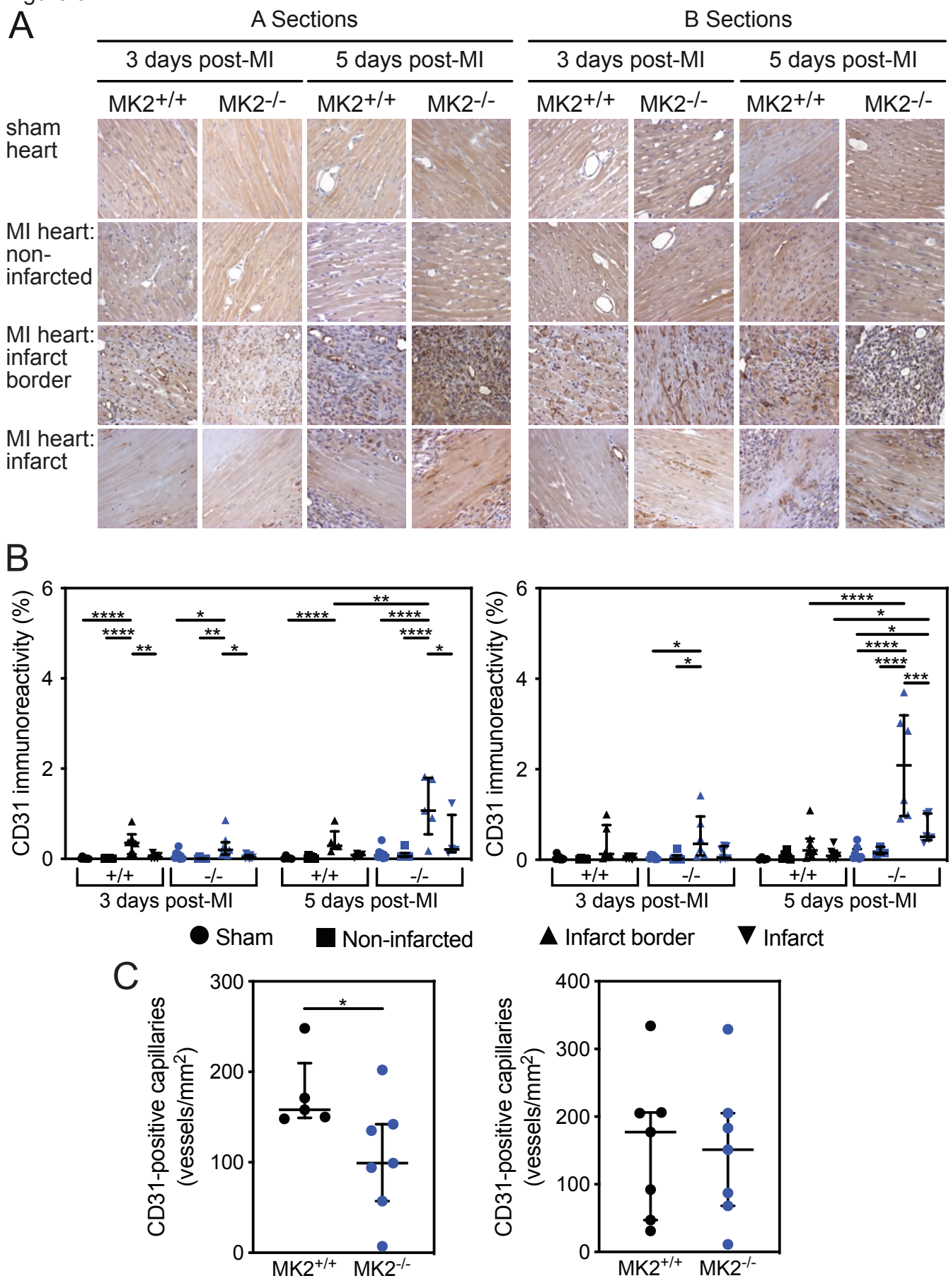

Figure 9

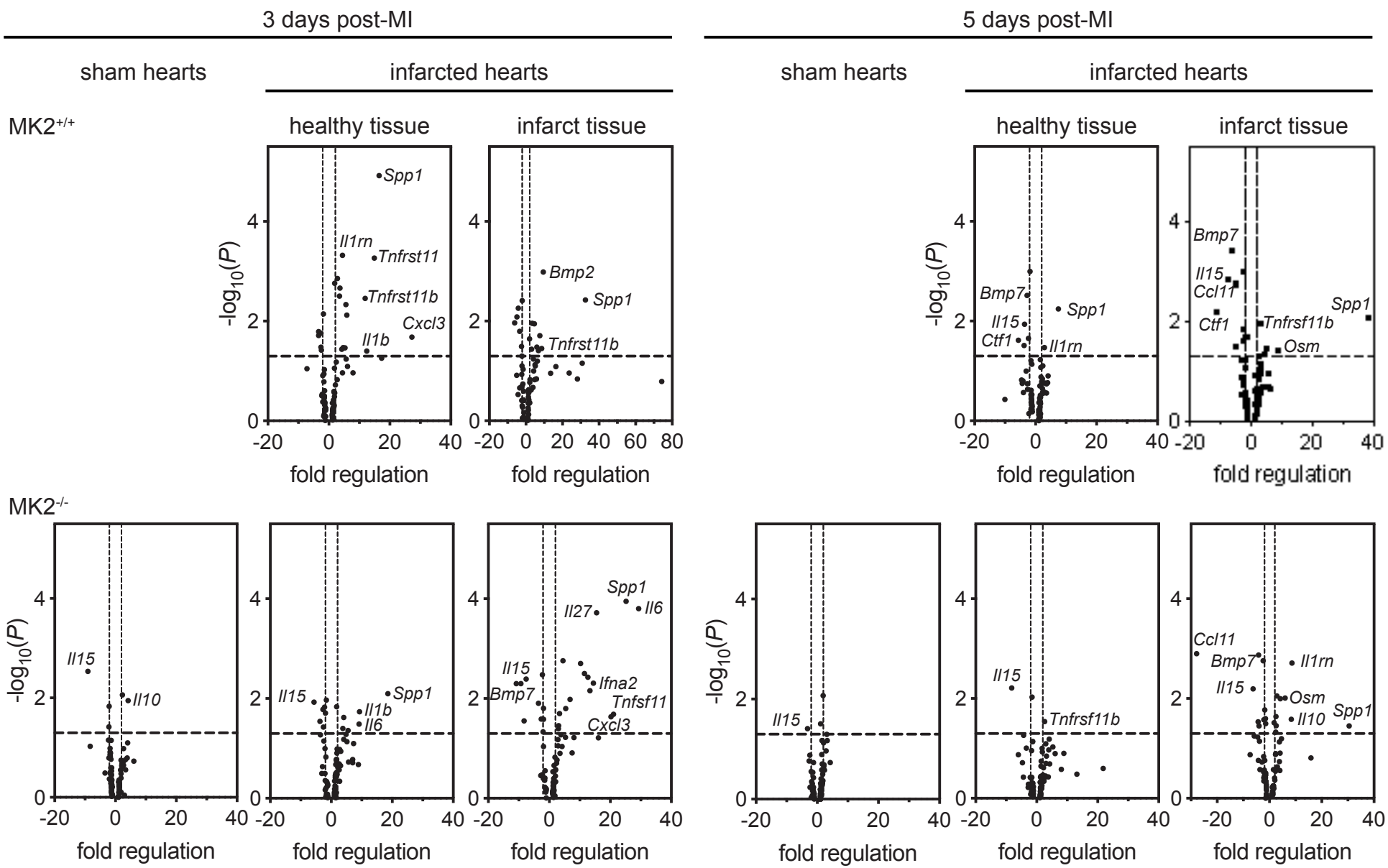
3 days post-MI
5 days post-MI
sham hearts
infarcted hearts
sham hearts
infarcted hearts
MK2+/+
healthy tissue
infarct tissue
healthy tissue
infarct tissue
MK2-/-
-log10(P)
fold regulation
Spp1
Il1rn
Tnfrst11
Tnfrst11b
Cxcl3
Il1b
Bmp2
Spp1
Tnfrst11b
Bmp7
Il15
Ccl11
Ctf1
Il1rn
Spp1
Tnfrsf11b
Osm
Il15
Il10
Il15
Spp1
Il1b
Il6
Spp1
Il6
Il27
Il15
Bmp7
Ifna2
Tnfsf11
Cxcl3
Il15
Tnfrsf11b
Ccl11
Bmp7
Il1rn
Il15
Osm
Il10
Spp1

Figure 10

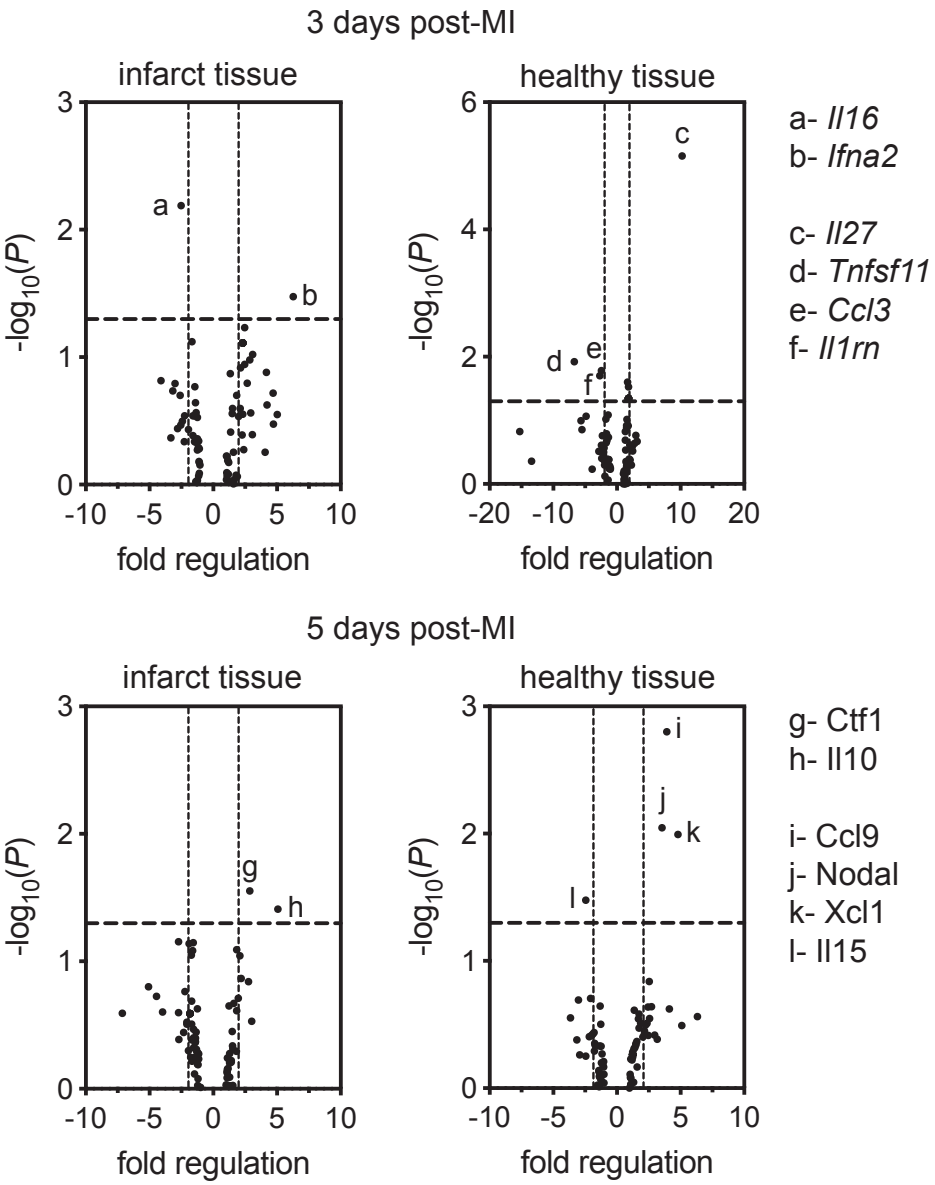

Figure 11